



1 Countrywide Digital Surface Models and Vegetation Height Models 2 from Historical Aerial Images

3 Mauro Marty¹, Livia Piermattei^{1,2}, Lars T. Waser¹, Christian Ginzler¹

4 ¹ Land Change Science Research Unit, Swiss Federal Institute for Forest, Snow and Landscape Research WSL, Birmensdorf,
5 8903, Switzerland

6 ²Department of Geography, University of Zurich, Zurich, 8057, Switzerland

7 *Correspondence to:* Mauro Marty (mauro.marty@wsl.ch)

8 **Abstract.** Historical aerial images, captured by film cameras in the previous century, are valuable resources for quantifying
9 Earth's surface and landscape changes over time. In the post-war period, these images were often acquired to create
10 topographic maps, resulting in the acquisition of large-scale aerial photographs with stereo coverage. Photogrammetric
11 techniques applied to these stereo images enable the extraction of 3D information to reconstruct digital surface models (DSMs)
12 and orthoimages.

13 Here, we present a highly automated photogrammetric approach for generating countrywide DSMs of Switzerland, at a 1 m
14 resolution, from approximately 40,000 scanned aerial stereo images acquired between 1979 and 2006, with known exterior
15 and interior orientation. We derived four countrywide DSMs for the epochs 1979–1985, 1985–1991, 1991–1998, and 1998–
16 2006. From the DSMs, we generated corresponding countrywide vegetation height models (VHMs). We assessed the quality
17 of the historical DSMs at the country scale and within six representative study sites, evaluating the vertical accuracy and the
18 completeness of image-matching across different land cover types.

19 Mean completeness ranged from 64% for 'glacial and perpetual snow' to 98% for 'sealed surfaces', with a value of 93% for
20 the 'closed forest' class. Across Switzerland, the median elevation accuracy of the historical DSMs compared with a reference
21 digital terrain model (DTM) on sealed surface points ranged from 0.28 to 0.53 m, with a normalised median absolute deviation
22 (NMAD) of around 1 m and a maximum root mean square error (RMSE) of 3.90 m. The same analysis between geodetic
23 points and historical DSMs showed higher accuracies, with median values of ≤ 0.05 m and an NMAD < 1 m.

24 The VHMs generated in this study enabled the detection of major changes in forest areas due to windstorm damage, forest
25 dynamics, and growth. This work demonstrates the feasibility of generating accurate, very high-resolution DSM time series
26 (spanning three decades) and VHMs from historical aerial images of the entire surface of Switzerland in a highly automated
27 manner. The VHMs are already being used to estimate countrywide biomass changes. The countrywide DSMs and VHMs for
28 the four epochs, along with auxiliary data, are available online at <https://doi.org/10.16904/envdat.528> (Marty et al., 2024) and
29 can be used to quantify long-term elevation changes and related processes across different surfaces.



30 **1 Introduction**

31 Photographs taken by film cameras on aeroplanes throughout the last century represent a unique and invaluable information
32 source for quantifying past changes in the Earth's surface and landscape. Various institutions and mapping agencies have
33 recognised this value by preserving and scanning these photographs and making them publicly available.

34 After the Second World War, large-scale aerial photographs were frequently taken to create topographic maps. To ensure
35 stereoscopic coverage and enable the extraction of three-dimensional (3D) information, image blocks were acquired in parallel
36 strips, with each photograph overlapping the next along the same flight line (forming a stereo pair). Due to the stereoscopic
37 acquisition and very high resolution of these images, digital surface models (DSMs) and orthoimages at a metric or sub-metric
38 resolution can be generated using digital photogrammetry and computer vision techniques. This capability has led to the use
39 of historical aerial images to assess long-term surface elevation changes across various geoscience fields.

40 Multi-temporal DSMs derived from historical aerial images have frequently been used in cryospheric research for assessments
41 of changes in glacier elevation (e.g., Magnússon et al., 2016; Belart et al., 2020; Denzinger et al., 2021), in periglacial studies
42 (e.g., Cusicanqui et al., 2021; Fleischer et al., 2021), in geomorphology (e.g., Micheletti et al., 2015; Piermattei et al., 2023;
43 Schwat et al., 2023), in volcanology (e.g., Gomez et al., 2015), in analyses of land-use change (e.g., Nebiker et al., 2014; Bolles
44 et al., 2018) and in archaeology (e.g., Risbøl et al., 2015; Peppas et al., 2018). Most studies have been focused on local scales
45 and have involved processing a small set of scanned aerial images, with a few considering larger scales (Geyman et al., 2022;
46 Muhammed et al., 2023) or even regional scales such as Greenland (Korsgaard et al., 2016).

47 In this study, we generated countrywide DSMs of Switzerland using historical aerial images acquired from the 1980s to the
48 early 2000s. Additionally, as we carried out the study within the framework of the Swiss National Forest Inventory (NFI), we
49 produced corresponding countrywide vegetation height models (VHMs). The Swiss NFI aims to collect objective information
50 on forests at the national level for scientific, political, social and economic purposes (Abegg et al., 2023). Data collection
51 within the context of the NFI is mainly based on a systematic terrestrial sample inventory, which is intended to provide results
52 for Switzerland as a whole, as well as for larger regions and individual cantons. Since the early days of the NFI, aerial image
53 interpretation and remote sensing data have been used. Over the decades, the image data has evolved from analogue black-
54 and-white images to digital RGB true colour aerial images, and finally to the digital colour infrared (CIR) sensor data used
55 today. In addition to the application of stereo-image-based analysis on various sample grids, comprehensive datasets have been
56 developed and produced.

57 The use of historical aerial images for 3D forest reconstruction is limited, with most studies focused on 2D changes in tree and
58 canopy cover at local scales using orthoimages (e.g., Kadmon and Harari-Kremer, 1999; Morgan and Gergel, 2010; Kulha et
59 al., 2018) and texture analysis (Hudak and Wessman, 1998; Kupidura et al., 2019). In Central Switzerland, Waser et al. (2008a,
60 b) used scanned colour infrared aerial images to generate DSMs and quantify tree/shrub cover changes between 1997 and
61 2002. Recent research has focused on methods based on artificial intelligence (AI) to extract information on woody vegetation
62 along alpine treeline ecotones, tree cover (Wang et al., 2022), and forest cover (Hufkens et al., 2020) from historical aerial

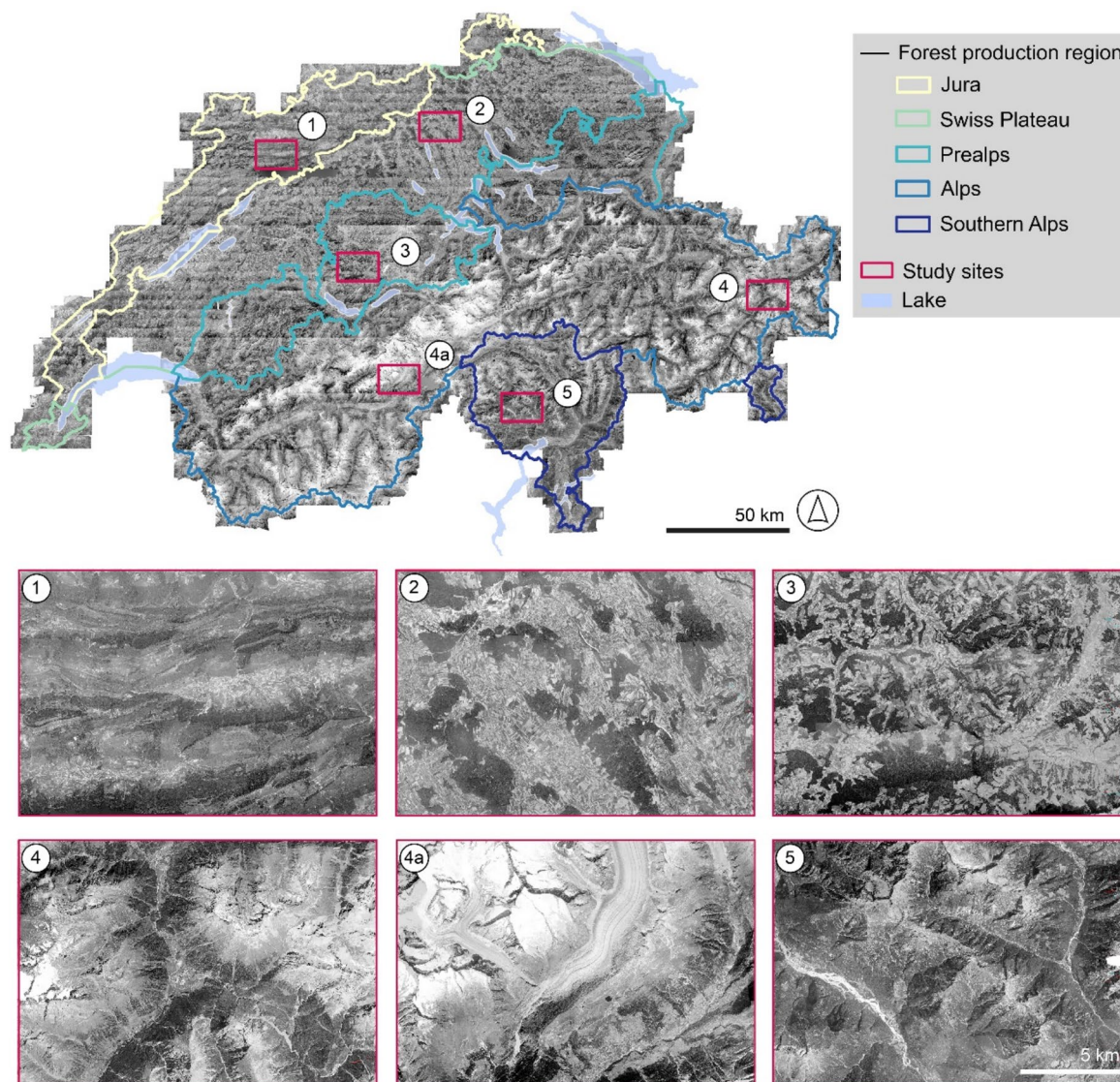


63 orthoimages. The study by Vége and St-Onge (2008) was among the first where forest canopy growth was quantified using
64 DSM time series from historical aerial images. As changes in the height of forest canopies over time represent a key aspect of
65 forest dynamics, further studies have been conducted to explore the use of historical images for tracking long-term changes in
66 canopy height (Nurminen et al., 2015; Božek et al., 2019; Hufkens et al., 2020) and forest stand age (Vastaranta et al., 2015)
67 and for describing the evolution of forest successional stages in tropical forests (Berveglieri et al., 2016, 2018).
68 Here, we present a highly automated approach to process scanned aerial images (hereafter referred to as ‘historical aerial
69 images’) for generating countrywide DSMs and VHMs in Switzerland. Expanding on the work by Heisig and Simmen (2021),
70 who generated a single countrywide orthoimage of Switzerland from images taken between 1985 and 1991, we processed all
71 scanned images available from swisstopo, the Swiss Federal Office of Topography (swisstopo, 2024a), acquired over
72 Switzerland between 1979 and 2006. Countrywide coverage was obtained using image acquisition intervals of approximately
73 seven years, leading to four countrywide DSM products for the epochs 1979–1985, 1985–1991, 1991–1998, and 1998–2006.
74 To derive VHMs, we normalised the elevation values from the historical DSMs by subtracting the available countrywide
75 digital terrain model (DTM; swissALTI3D version 2017, swisstopo). We assessed the quality of the generated DSMs by
76 evaluating the completeness of the image-matching process across different land cover types and the vertical accuracy of the
77 historical DSMs by comparing elevation values with: (i) the reference DTM, (ii) geodetic elevation points on a national scale,
78 and (iii) manual stereoscopic elevation measurements from six representative study sites in Switzerland. We close the article
79 by highlighting the potential applications of these datasets in research on forest dynamics and management.

80 **2 Dataset and methods**

81 **2.1 Historical aerial stereo imagery of Switzerland**

82 DSMs and VHMs were generated from historical images covering the entire 41,285 km² of Switzerland, with an elevation
83 range between 197 and 4634 m a.s.l. In the Swiss NFI, Switzerland is characterised by different types of landscapes and is
84 divided into five main forest production regions: the Jura in the northwest (1), the Swiss Plateau (2), the Prealps (3) between
85 the Swiss Plateau and the Alps, the Alps (4/4a), and the Southern Alps (5) (Fig. 1). These regions exhibit different climatic
86 and topographic characteristics, such as land cover classes, elevation ranges, tree species and forest structures (Tab. 1).
87 Representative study sites of approximately 210 km² (i.e., one map sheet; see section 2.2.2) were selected within these regions
88 (Fig. 1). In the Alps region, an additional study site encompassing the tongue of the Grosser Aletsch Glacier was included.
89 The data used to generate the DSMs consists of approximately 40,000 panchromatic images acquired with an RC10 aerial
90 camera manufactured by Wild Heerbrugg (currently owned by Leica Geosystems, Heerbrugg, Switzerland). Multiple airborne
91 campaigns were conducted from 1979 to 2006, with each campaign spanning approximately seven years to cover the entire
92 country. The first countrywide coverage was obtained from the acquisition campaign that took place between 1979 and 1985
93 (epoch 1), followed by subsequent campaigns from 1985 to 1991 (epoch 2), 1991 to 1998 (epoch 3), and 1998 to 2006 (epoch
94 4) (Fig. 2).



95

96 **Figure 1: The Swiss NFI forest production regions (1 = Jura, 2 = Swiss Plateau, 3 = Pre-Alps, 4 = Alps, 5 = Southern Alps) in**
97 **Switzerland and the respective location of the study site for each region, along with the generated orthoimage for epoch 1 (1979–**
98 **1985). An additional study site (4a) was selected for the Alps forest production region.**

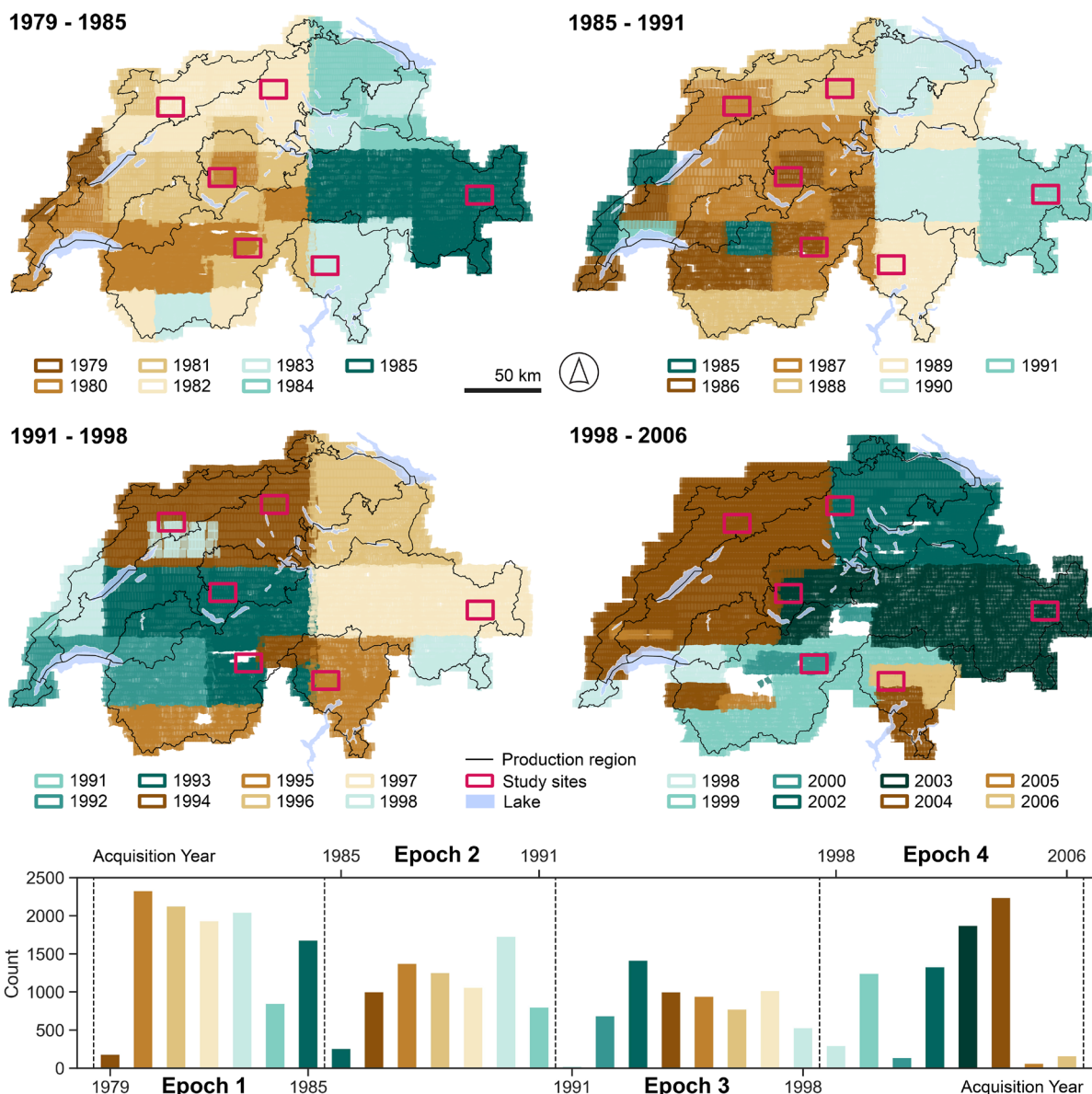
99 The primary purpose of these photograph acquisitions was to update the topographic maps produced by swisstopo. The
100 photographs were acquired with approximately 70–80% front overlap and 30–40% side overlap. The average flight height for
101 all datasets was approximately 4,000 m above the ground, with an image scale of about 1:25,000. The photographs were
102 scanned with a resolution of 14 μm using a Leica DSW700 scanner (swisstopo). This resulted in an average ground sample
103 distance (GSD) of around 0.35 m in the scanned images, with larger variations in high-elevation areas. Historical aerial images
104 are freely available on swisstopo's website (swisstopo, 2024a) and are provided with exterior orientation parameters, as well



105 as camera calibration protocols containing interior orientation parameters such as focal length and fiducial mark values. Figure
 106 2 shows the image footprints of the stereo pairs used to generate the DSMs, along with the corresponding year of acquisition.

107 **Table 2: Forest production region characteristics. Topographic parameters are based on the swissALTI3D digital terrain model**
 108 **(DTM) version 2017. Forest parameters are based on the Swiss National Forest Inventory (NFI).**

Forest production region		Area (km ²)	Elevation range (m a.s.l.)	Mean slope (°)	Forest cover (%)	Forest type			
No.	Name					pure coniferous (%)	mixed coniferous (%)	mixed deciduous (%)	pure deciduous (%)
1	Jura	4935.4	244–1677	12.3	39.5	28.6	25.5	18.8	22.3
2	Swiss Plateau	9412.8	311–1685	7.2	24.2	37.8	22.9	13.6	22.1
3	Prealps	6608.1	370–2899	19.8	32.5	53.7	22.4	8.2	9.6
4	Alps	16782.6	370–4634	28.9	21.0	71.0	9.6	5.8	8.6
5	Southern Alps	3545.7	192–3899	31.6	39.2	31.7	7.4	5.2	51.9



109

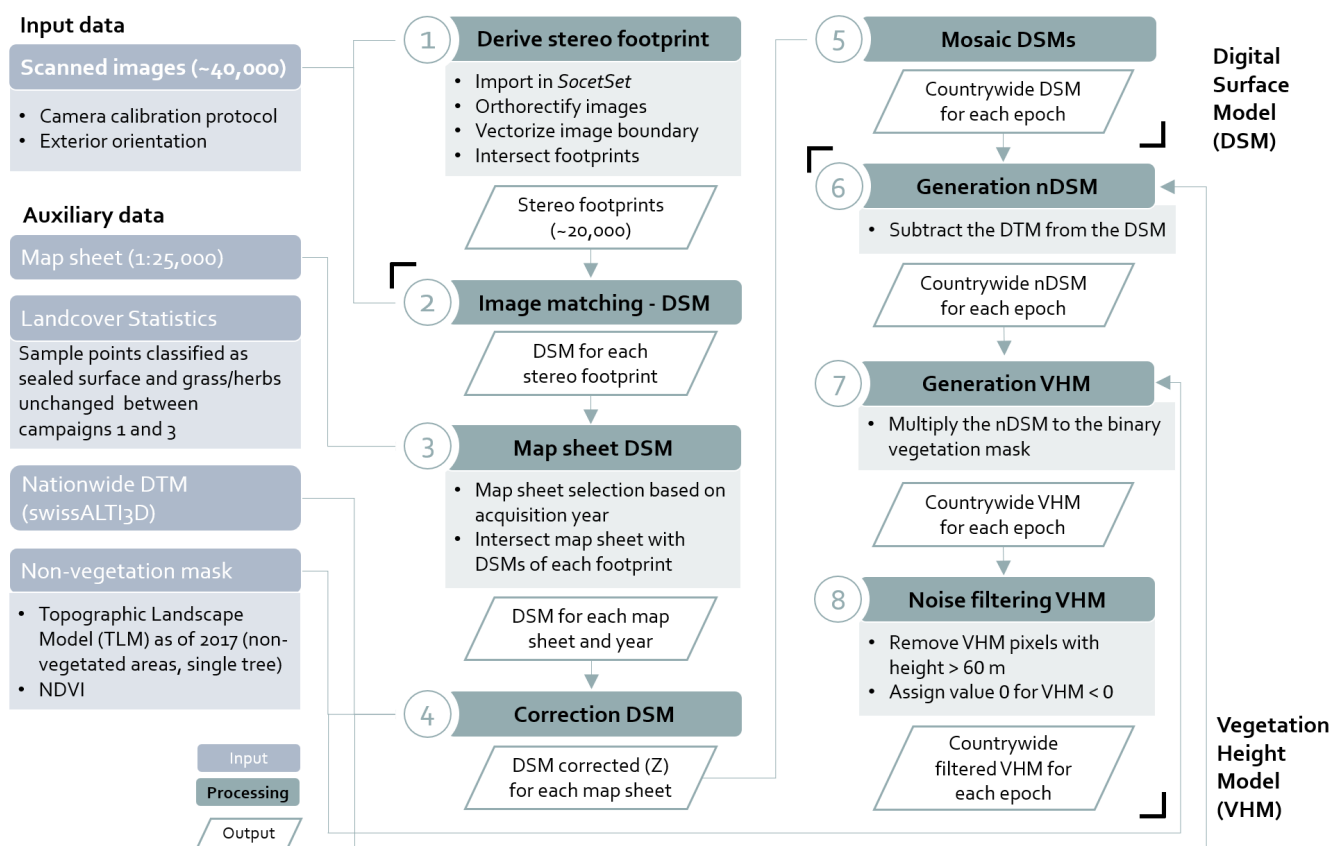
110 **Figure 2: Stereo footprint coverage over Switzerland for the four epochs and the number of images used for the respective digital**
 111 **surface model (DSM) generation (barplot, bottom). There is an overlap of acquisition years between adjacent epochs, but images**
 112 **from the same year cover different forest production regions in each epoch.**

113 2.2 DSM and VHM generation

114 The scanned input images, auxiliary data, and the steps used to generate the DSMs and the VHMs are illustrated in Fig. 3. The
 115 countrywide DSMs and VHMs are provided at 1 m spatial resolution in the Swiss projected coordinate system CH1903+ /
 116 LV95 (EPSG code 2056), and height information is supplied in LN02 (EPSG code 5728) where applicable. The scanned
 117 historical images were processed using the commercial photogrammetric software SocetSet (v5.6.0) by BAE Systems (Falls



118 Church, USA). With known interior and exterior orientation parameters, DSMs can be generated using the Next-Generation
 119 Automatic Terrain Extraction (NGATE) package implemented in SocetSet (DeVenecia et al., 2007). The exterior orientation
 120 information for the images from epochs 1, 2 and 4 was derived by swisstopo within the framework of the Swiss Land
 121 Use/Cover Statistics program around 2004. Image orientation was performed using ground control points (GCPs), visible in
 122 the historical imagery, and in more recent already-oriented digital stereo images available from swisstopo. The elevation of
 123 the GCPs was stereoscopically extracted from the digital images. This image orientation resulted in accurate horizontal
 124 positioning but biases in the Z direction, ranging from 1 to 5 m, randomly distributed across Switzerland. Therefore, the DSMs
 125 from these epochs were vertically corrected, as described in section 2.2.2. In contrast, the images for epoch 2 were recently
 126 oriented using a highly automated workflow, as described by Heisig and Simmen (2021).



127
 128 **Figure 3: Workflow of historical image processing and countrywide digital surface model (DSM) and vegetation height model (VHM)**
 129 **generation.**

130 2.2.1 Image-matching and DSMs

131 The DSM generation process using the NGATE package followed a highly automated workflow. To handle the DSM
 132 reconstruction process for approximately 40,000 images, image-matching was performed on distributed machines for single



133 stereo footprints (i.e., stereo pairs). In the initial step, the footprint for each image was calculated, and the footprints of adjacent
134 images along the same flight line were intersected to create stereo footprints. In total, 20,346 stereo footprints were processed.
135 All stereo footprints were stored in a table on a PostGIS database, which was used to control the image-matching process
136 running on distributed virtual machines. Since stereo pairs were formed only from the neighbouring images along the same
137 flight line, multi-image-matching was not involved in this process.
138 NGATE provides several predefined correlation/matching strategies for different types of image content, such as urban, flat
139 and low-contrast areas. To ensure the extraction of accurate and complete elevation information across different land cover
140 types, two strategies were adopted, namely urban and low contrast. The urban strategy utilises internal correlation parameters
141 that account for elevation discontinuities, while the low-contrast strategy aims to identify congruent points on highly
142 homogeneous surfaces. While image-matching in NGATE is conducted on every pixel of the input imagery, the resulting
143 output file represents a regular grid of three-dimensional (XYZ) coordinates. Optionally, this grid can include information
144 about successful image-matching or interpolation for the given pixel, as indicated by the Figure of Merit value, a product
145 derived by the software. The spatial resolution of the output DSM is user-defined and, in our case, was set to 1 m, approximately
146 three times the GSD of the scanned images.
147 The image-matching using the two strategies resulted in two separate DSMs for each stereo footprint. These two DSMs were
148 combined into one DSM by including all successfully matched points from the urban strategy, as forests typically exhibit large
149 elevation discontinuities. Any remaining gaps in this DSM were filled with correlated points from the low-contrast strategy,
150 where available.

151 **2.2.2 DSM merging and vertical correction**

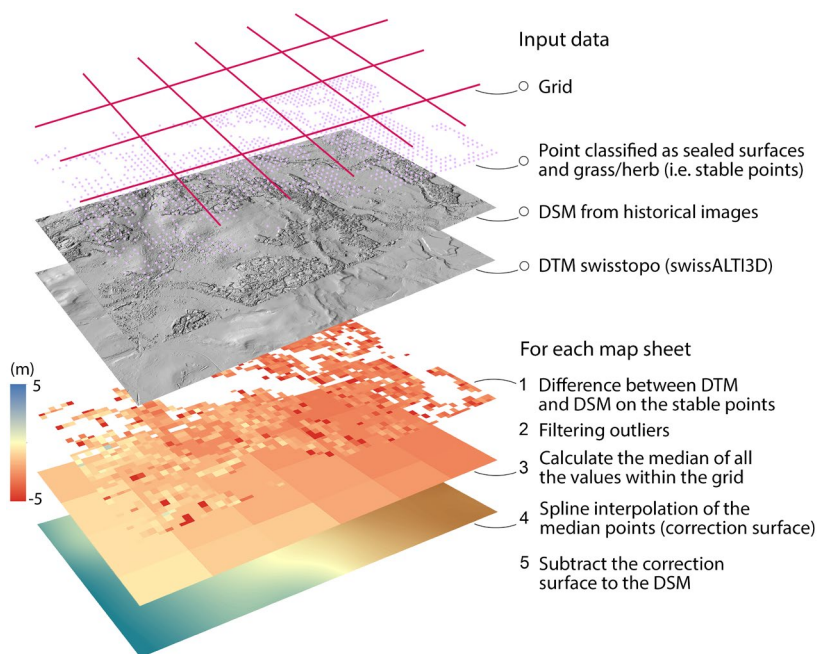
152 The exterior orientation of the images from epochs 1, 3 and 4 resulted in a vertical offset of up to 5 m between the DSMs and
153 the reference DTM on stable terrain (i.e., sealed surfaces and grass/herb points; see section 2.3.1). Therefore, the DSMs from
154 these epochs were vertically corrected. For consistency, this correction was also applied to the DSM from epoch 2, resulting
155 in neglectable changes due to the already precise horizontal and vertical orientation.

156 The correction of approximately 20,000 DSMs of single stereo footprints was performed at the level of 1:25,000 map sheet
157 units, provided by swisstopo (swisstopo, 2024b). These map sheets were originally used to plan airborne image acquisition
158 campaigns. For each map sheet geometry, all DSMs of single stereo footprints belonging to the same epoch were selected via
159 spatial intersection, merged and cut to the map sheet extent (approximately 50 stereo footprints in flat areas and up to 150 in
160 high-alpine regions). Since adjacent stereo footprints always overlapped spatially, pixels on these locations often included
161 multiple elevation values, which were generalised using the median height. Grid cells without any successfully matched
162 elevation information were interpolated using a triangular irregular network (TIN) surface.

163 The vertical correction of the generated DSM for each map sheet and epoch is illustrated in Fig. 4. The workflow consisted of
164 calculating the difference between the reference DTM (swissALTI3D version 2017; see section 2.2.3) and the generated DSM
165 at points corresponding to the classes ‘sealed surface’ and ‘grass/herb’ in the first and third campaigns of the Swiss Land



166 Use/Cover Statistics program (1979–1985 and 2004–2009, respectively; see section 2.3.1). With this approach, only points
167 with an unchanged land cover classification were used. Outliers were filtered out based on mean ± 1 standard deviation (Std),
168 calculated in a 50×50 pixel moving window. The median of the remaining elevation differences for each of the 1200 regular
169 grid cells per map sheet was then calculated. Finally, a coarse correction surface (spline interpolation) was derived from these
170 median values and applied to the resulting DSMs at the map sheet unit level to correct elevation bias.



171
172 **Figure 4: Illustration of the workflow to correct the elevation bias in the historical digital surface models (DSMs) for each map sheet.**
173 **The correction is based on the elevation difference between the reference digital terrain model (DTM) and the historical DSM for**
174 **sample points classified as grass/herb or sealed surfaces.**

175 2.2.3 Countrywide DSMs and VHMs

176 After randomly distributed elevation biases (section 2.2.2) were corrected in each map sheet DSM of each epoch, the individual
177 map sheet DSMs were combined into one DSM as a Geotiff file, covering the whole of Switzerland.

178 The four countrywide VHMs were derived by calculating the difference between the historical DSMs and the reference DTM
179 (swissALTI3D version 2017, swisstopo; see workflow in Fig. 3). This process resulted in a normalised DSM (nDSM),
180 representing the heights of all existing objects above ground. Note that the reference DTM was resampled from the default
181 resolution of 2 m to 1 m to match the resolution of the generated DSMs. The swissALTI3D DTM is based on airborne laser
182 scanning data for elevations up to 2000 m a.s.l., with an overall point density of 0.5 points/m² and a vertical accuracy of ± 0.5
183 m (standard deviation). Above 2000 m a.s.l., elevation information is derived by image-matching and manual editing, yielding
184 a documented vertical accuracy of 1–3 m on average (swisstopo, 2024c).



185 nDSM raster cells with values > 60 m were considered outliers due to erroneous image-matching and thus were replaced by
186 'no data'. Next, the VHM (i.e., the nDSM of vegetated areas) was generated by assigning a height above ground of 0 m to all
187 non-vegetated objects. To achieve this, a binary non-vegetation mask (0 = non-vegetation and 1 = vegetation) was created by
188 combining information from the topographic landscape model (TLM; swisstopo, 2024d) and a normalised difference
189 vegetation index (NDVI) map obtained from aerial orthoimages of the years 2009–2015. All areas classified in the TLM as
190 building, street, and water surface, as well as pixels with an NDVI < 0.1 , were set to 0. To retain vegetation close to buildings
191 and streets in the VHMs, single trees and hedges from the TLM were buffered by 15 m and set to 1. This non-vegetation mask
192 was multiplied by the nDSMs. The resulting VHMs had a spatial resolution of 1 m, consistent with the historical DSMs.

193 **2.3 Quality assessment of the DSMs**

194 The quality of the generated DSMs was assessed by analysing: (1) the completeness achieved through the image-matching
195 process over different land cover types and (2) the elevation accuracy based on elevation differences to reference datasets (see
196 section 2.3.1). The elevation differences were calculated consistently as the reference data minus the historical DSMs.
197 Therefore, positive differences indicated that historical DSMs had negative biases, i.e., that the reference data was higher than
198 the historical DSM. Quality assessment was performed and reported for the six selected areas and the countrywide DSMs.

199 **2.3.1 Reference data**

200 The reference dataset used to assess the completeness of the image-matching process over different land cover classes consisted
201 of sample point interpretation on a regular 100 m grid across Switzerland. These sample points were collected by the Swiss
202 Federal Statistical Office in the framework of the Swiss Land Cover/Use Statistics program (BFS, 2024) (Fig. A1). These
203 countrywide land cover statistics campaigns took place in 1979–1985, 1992–1997, 2004–2009 and 2013–2018. The
204 completeness for epoch 1 was assessed, and the reference data from the 1979–1985 campaign was used. This dataset comprised
205 121,896 points for the 6 selected areas. The 27 specific land cover classes were grouped into 6 categories: (1) sealed surface,
206 (2) bare land, (3) grass/herb, (4) shrub, (5) closed forest, and (6) glacial and perpetual snow.

207 The vertical accuracy of the DSMs was assessed by comparing the elevation with three reference datasets. First, the sealed
208 surface points that remained unchanged between the 1979–1985 and 2004–2009 campaigns were used. At these points, the
209 elevation differences between the reference DTM and the DSMs were calculated. The reference DTM was the same as the one
210 used for generating the VHM (see section 2.2.3).

211 The second dataset comprised 565 selected geodetic control points (i.e., measured with GNSS or triangulation) distributed
212 throughout Switzerland. This dataset is monitored and maintained by swisstopo; the documented vertical accuracy ranges from
213 0.003 to 0.1 m, with 42% of the points showing accuracies of 0.05 m or better. For the remaining ones, an accuracy of 0.1 m
214 is documented (swisstopo, 2023). These geodetic points enabled a completely independent estimation of the vertical accuracy
215 of the derived DSMs.



216 As a third reference dataset, 16,650 stereoscopic elevation measurements conducted by a stereo-image interpreter at the Swiss
217 Federal Institute for Forest, Snow and Landscape Research (WSL) were used. The data collection scheme was the same as in
218 the NFI (Ginzler, 2019). These measurements were derived only for epoch 1 and within the 666 forest plots of 50×50 m area
219 intersecting the 6 study sites (Fig. 1). For each forest plot, 25 elevation measurements were extracted on the same stereo pair
220 as used for generating the historical DSM (Fig. A1). In addition, the six land cover classes used to assess completeness were
221 assigned to each stereo measurement. The ‘closed forest’ land cover class was further divided into coniferous or deciduous
222 trees.

223 **2.3.2 DSM completeness**

224 Completeness is an essential quality measure for photogrammetric DSM generation. Here, it was computed as the percentage
225 of successfully matched points out of the potential total number of matched points within a defined spatial unit. Completeness
226 was calculated within circles with a radius of 5 m centred around points of the land cover statistics dataset. Then, the mean
227 completeness was calculated for the six land cover classes (i.e., sealed surface, bare land, grass/herb, shrub, closed forest, and
228 glacial and perpetual snow). Completeness values were calculated in the six study sites for all four epochs.

229 **2.3.3 Vertical accuracy**

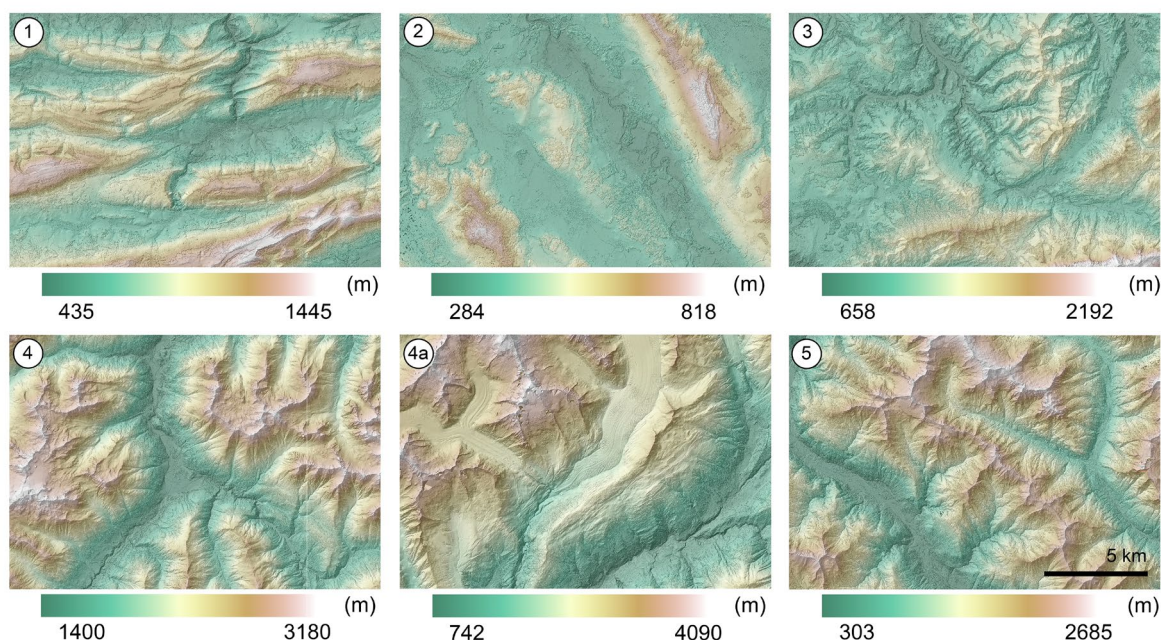
230 Vertical accuracy was calculated as the difference between the reference dataset (see section 2.3.1) and the DSMs. First, the
231 elevation differences between the reference DTM and the DSMs were calculated at points classified as sealed surfaces. In
232 addition, points classified as grass/herb and bare land were used to quantify the elevation bias of the DSMs to terrain slope,
233 aspect and elevation. Sealed surface points were not used in this investigation because they were mainly located in flat areas.
234 In a second analysis, the elevation values of the DSMs were compared with approximately 500 independent geodetic points.
235 Finally, > 16,000 stereoscopic elevation measurements were used to assess the performance of the image-matching workflow
236 on deciduous and coniferous trees, the primary target objects. It is worth noting that this latter comparison was used to evaluate
237 agreement rather than serving as a measure of accuracy, since the stereoscopic measurements have some inherent inaccuracies.
238 To calculate the statistical measures, differences greater than ± 50 m between the reference measurements and DSMs were
239 excluded because such values indicated a failure in image-matching due to cloud cover or saturated images, yielding unrealistic
240 elevation values. From the remaining differences, robust statistics, such as the median and the normalised median absolute
241 deviation (NMAD) were calculated, as biases in spatial datasets are often not normally distributed (Höhle and Höhle, 2009).
242 The NMAD is defined as $1.4826 \cdot \text{MAD}$ (mean absolute deviation). Root mean square error (RMSE) values were additionally
243 calculated, as a standard quality metric to facilitate the comparison of our results with those from other studies. RMSE values
244 were determined after applying outlier removal (mean ± 3 Std).



245 3 Results

246 3.1 Generation of DSMs

247 Four countrywide DSMs were generated successfully with the NGATE package of SocetSet. Data voids are related to the lack
248 of stereo images (Fig. 2) or to unsuccessful image-matching in saturated or cloudy areas. Figure 5 shows the hillshaded DSM
249 for the epoch 1979–1985 for the six study sites.



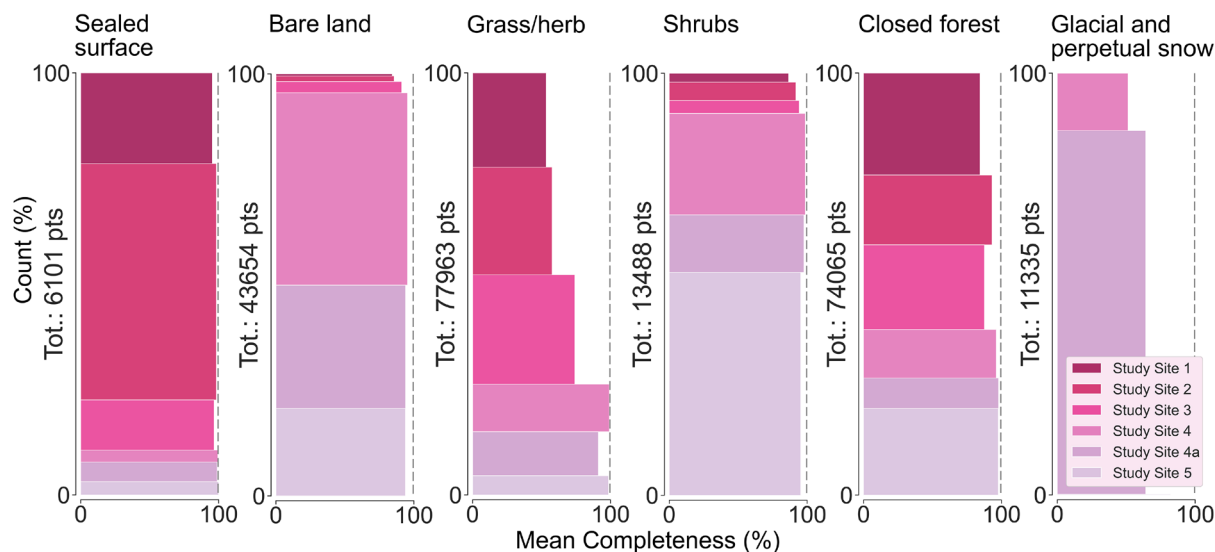
250

251 **Figure 5: Hillshaded digital surface models (DSMs) for the six selected study sites and epoch 1 (1979–1985). The year of the DSM is**
252 **1982 for sites 1 and 2, 1980 for site 3, 1985 for sites 4 and 4a, and 1983 for site 5.**

253 3.2 DSM completeness

254 Figure 6 shows the DSM completeness percentages for epoch 1 and the six land cover classes: sealed surface, bare land,
255 grass/herb, shrub, closed forest, and glacial and perpetual snow. The number of sample points for each class is also provided
256 in the figure. Completeness results for epochs 2, 3 and 4 are provided in Appendix A (Fig. A2), and Table A1 shows the
257 corresponding mean values. The lowest completeness occurred in areas classified as glacial and perpetual snow, with a mean
258 completeness of 65% across the four epochs. This result was expected, due to the textureless black-and-white images of these
259 surfaces, which resulted in poor image-matching performance. The highest completeness was achieved for sealed surfaces,
260 with a mean of 98%. For the classes bare land, shrub and closed forest, the mean completeness was approximately 90%,
261 whereas the grass/herb class had a mean of 79%. However, the completeness for the grass/herb class was higher for epochs 2,
262 3 and 4 (Fig. A2), with a minimum value of 84%.

263



264

265 **Figure 6: Distribution of the mean completeness values (as percentages) for epoch 1 across the six study sites and the six land cover**
266 **classes – sealed surface, bare land, grass/herb, shrub, closed forest, and glacial and perpetual snow. The snow class is only present**
267 **in study sites 4, 4a and 5. Note that for some classes and study sites, the number of points is minimal. For example, there are only 18**
268 **points in study site 5, which is equivalent to 0.15% for the class ‘glacial and perpetual snow’, and therefore the horizontal bar is not**
269 **visible.**

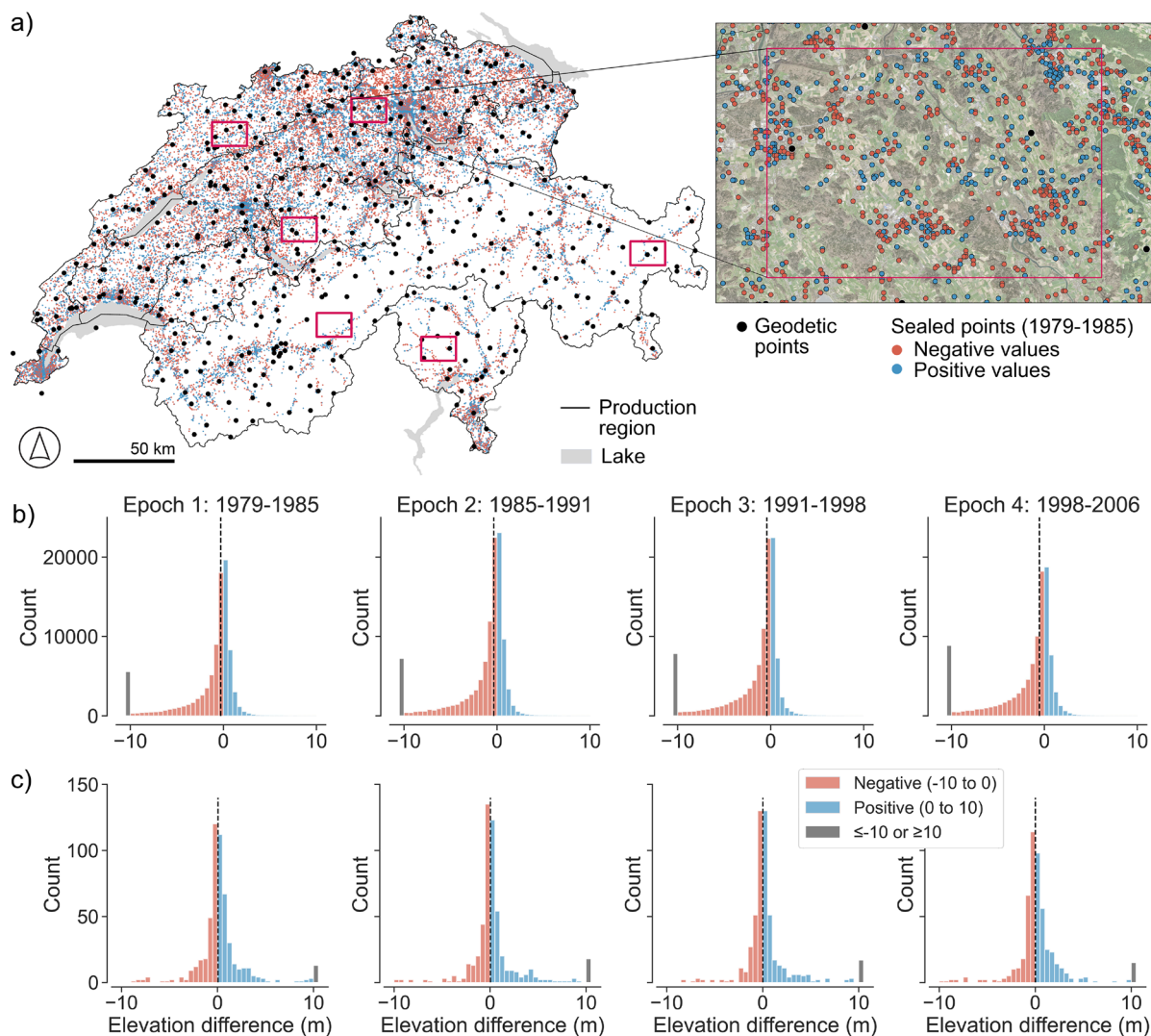
270 3.3 DSM vertical accuracy assessment

271 The vertical accuracy of the DSMs for each epoch was assessed by comparing them with three reference elevation datasets
272 (see section 2.3.1). Figure 7a shows the spatial distributions of the sealed surface points and the reference geodetic points,
273 while Table 2 summarises the statistical measures. Sealed surface points exhibit a clustered distribution in low-elevation areas
274 (i.e., regions 1, 2 and 3) and a sparser distribution in the Alps and Southern Alps (regions 4 and 5, respectively). No clear
275 systematic difference is observed when visualising the positive and negative elevation differences at sealed surface points
276 between the DTM and the DSM from the first epoch. However, plotting the frequency distribution of elevation differences
277 across the entire country reveals a negatively skewed distribution for all epochs (Fig. 7b). Negative differences, where the
278 reference DTM is lower than the historical DSM, may result in the suboptimal location of sealed surface points close to the
279 urban area and forest edge, which could explain the presence of several values < -10 m. The negative skew is also reflected in
280 the median values of the elevation differences (Table 2), with values between -0.3 and -0.5 m and an NMAD of approximately
281 1.5 m.

282 In the analysis of the vertical accuracy of the DSMs in comparison to independent geodetic points, the median is around zero,
283 with an NMAD of < 1 m (Table 2). Note that the number of geodetic points is two orders of magnitude smaller than the sealed
284 surface points and more evenly distributed over the country. Additionally, the number of geodetic points varies slightly across
285 the different epochs due to the spatial coverage of the image-matching results (e.g., cloud cover and image saturation). The



286 differences between the geodetic points and DSMs have a more symmetric distribution for all four epochs, with few positive
 287 differences > 10 m (Fig. 7c).



288
 289 **Figure 7: (a) Spatial distribution of the sealed surface points and the geodetic points used for the vertical accuracy assessment of the**
 290 **historical digital surface models (DSMs). Sealed surface points are depicted in blue and red, representing the positive and negative**
 291 **differences, respectively, between the reference digital terrain model (DTM) and the DSM for epoch 1. The inset shows the**
 292 **distribution of the sealed surface points and the geodetic points for study site 2, overlaid on the orthophoto for the year 2021**
 293 **(swisstopo, 2023). Frequency distributions of the elevation difference in metres between the DTM (swissALTI3D) and the DSM (b)**
 294 **on sealed surface points and (c) on geodetic points for the whole of Switzerland for the four epochs. The vertical dashed line indicates**
 295 **the median value. The bin size is 0.5 m.**

296
 297
 298

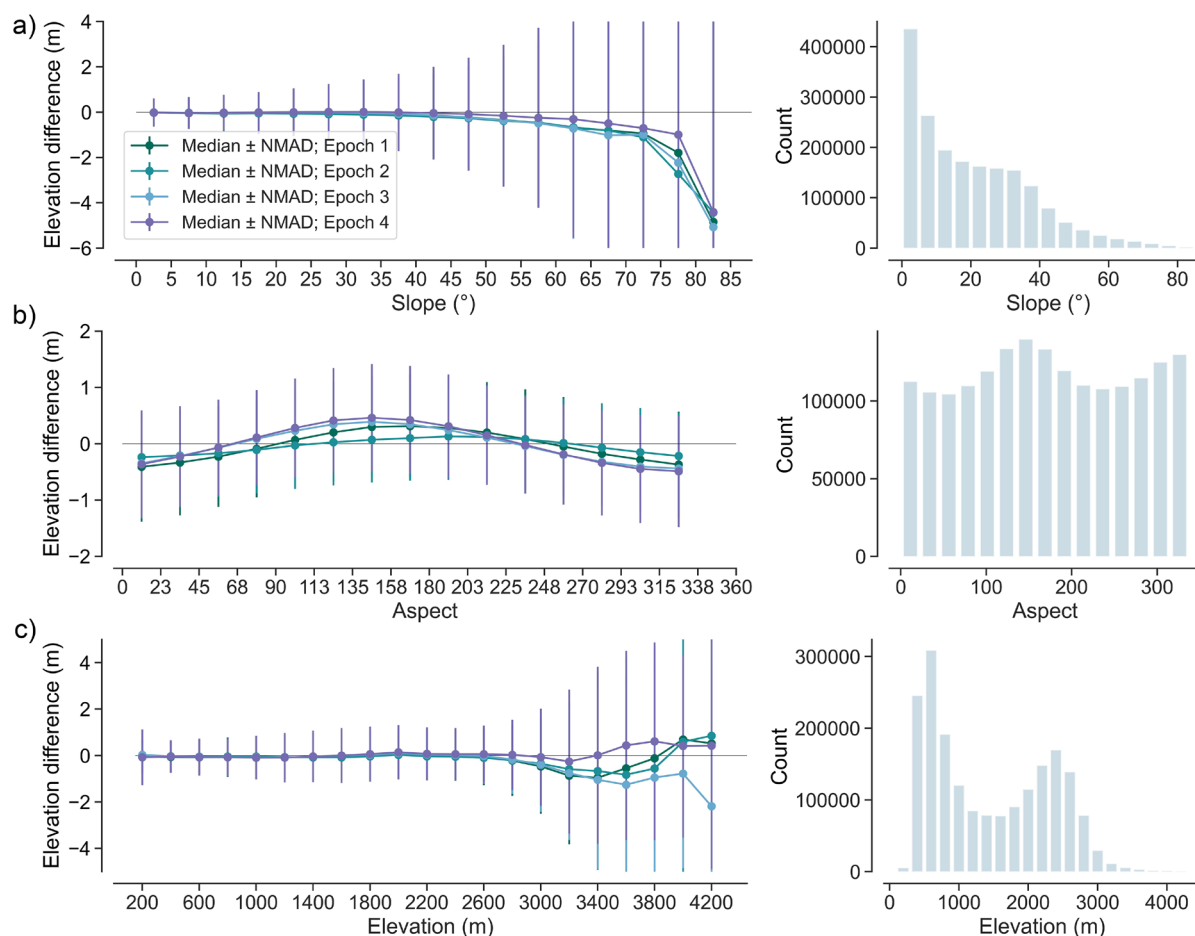


299 **Table 2: Elevation difference between the digital terrain model (DTM) and the historical digital surface models (DSMs) over the**
 300 **sealed surface points and the geodetic points over Switzerland for the four epochs. The number of points before and after outlier**
 301 **filtering is reported; the latter number was used for the root mean square error (RMSE) calculation.**
 302

Epochs	Accuracy on sealed surface points					Accuracy on geodetic points				
	No. points (±50 m)	Median (m)	NMAD (m)	No. points after filter (± 3 Std)	RMSE (m)	No. points (±50 m)	Median (m)	NMAD (m)	No. points after filtering (± 3 Std)	RMSE (m)
Epoch 1	90509	-0.28	1.08	86993	2.98	551	0.05	0.96	532	2.75
Epoch 2	111761	-0.35	1.11	107496	3.12	542	0.03	0.82	526	3.25
Epoch 3	108358	-0.41	1.14	104032	3.40	536	0.02	0.78	517	2.91
Epoch 4	102338	-0.53	1.41	98157	3.90	525	0.00	0.98	509	3.33

303
 304 The elevation difference between the DTM and the historical DSMs over grass/herb and bare land points shows no significant
 305 bias with slope, aspect or elevation, as shown in Figure 8. However, for elevations above 3000 m a.s.l. and slopes greater than
 306 45°, the NMAD increases drastically, exceeding 2 m for all four countrywide DSMs. However, points within these intervals
 307 represent only approximately 5% (slope) and 1% (elevation), as shown in the histograms in Fig. 8. The elevation bias
 308 dependence on aspect shows a potential shift, with median values below 0.5 m and a constant NMAD of ± 0.8 m for all datasets
 309 and aspect intervals.

310 The agreement between the stereoscopic measurement (see section 2.3.3) taken within the NFI plots and the historical DSM
 311 of epoch 1 is reported in Table 3 for the different land cover classes, including a division of the closed forest class into
 312 deciduous and coniferous trees. Figure 9 shows one NFI plot with the stereo measurement location and elevation values
 313 compared with the DSM profile. As shown in Table 3, the closest agreement is observed for the sealed surface class, with a
 314 median difference of 0.19 m and an NMAD of 0.63 m, comparable to the results obtained when analysing the difference
 315 between the DTM and DSM for this land cover class (see Table 2). For the grass/herb class, the differences to the stereo
 316 measurements exhibit a similar offset but with a larger spread, with a median of -0.15 m and an NMAD of about 1 m. Sample
 317 points from the shrub and bare land classes show a wider spread, with NMAD values of 1.62 m and 1 m, respectively, and
 318 larger systematic biases, with median values greater than -0.4 m. The weakest agreement is found for the closed forest class,
 319 where deciduous and coniferous trees yield comparable results, with median values of about -1.8 m and NMAD values of up
 320 to 3.77 m.

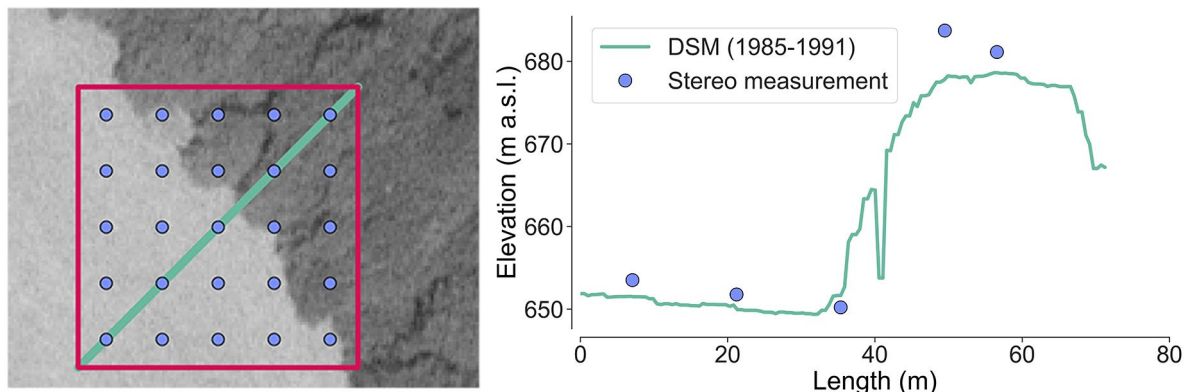


321

322 **Figure 8: Elevation differences in grass/herb and bare land points as a function of slope (a), aspect (b), and elevation (c). The**
 323 **histogram on the right shows the number of points for each interval. Elevation differences are calculated as the reference digital**
 324 **terrain model (DTM) minus historical digital surface models (DSMs). Slope, aspect and elevations were derived from the reference**
 325 **DTM.**

326 **Table 3: Elevation differences over different land cover classes between stereo measurements and the historical digital surface model**
 327 **(DSM) from epoch 1.**

Land cover class	No. points	Median (m)	NMAD (m)	No. points after filtering (± 3 Std)	RMSE (m)
Closed forest, deciduous trees	2917	-1.83	2.75	2855	4.35
Closed forest, coniferous trees	2478	-1.77	3.77	2441	5.47
Grass/herb	6792	-0.15	1.02	6634	1.6
Shrub	424	-0.41	1.62	415	2.35
Sealed surfaces	408	0.19	0.63	401	1.24
Bare land	1231	-0.74	1.00	1219	1.43
Glacial and perpetual snow	567	0.17	2.15	540	2.99

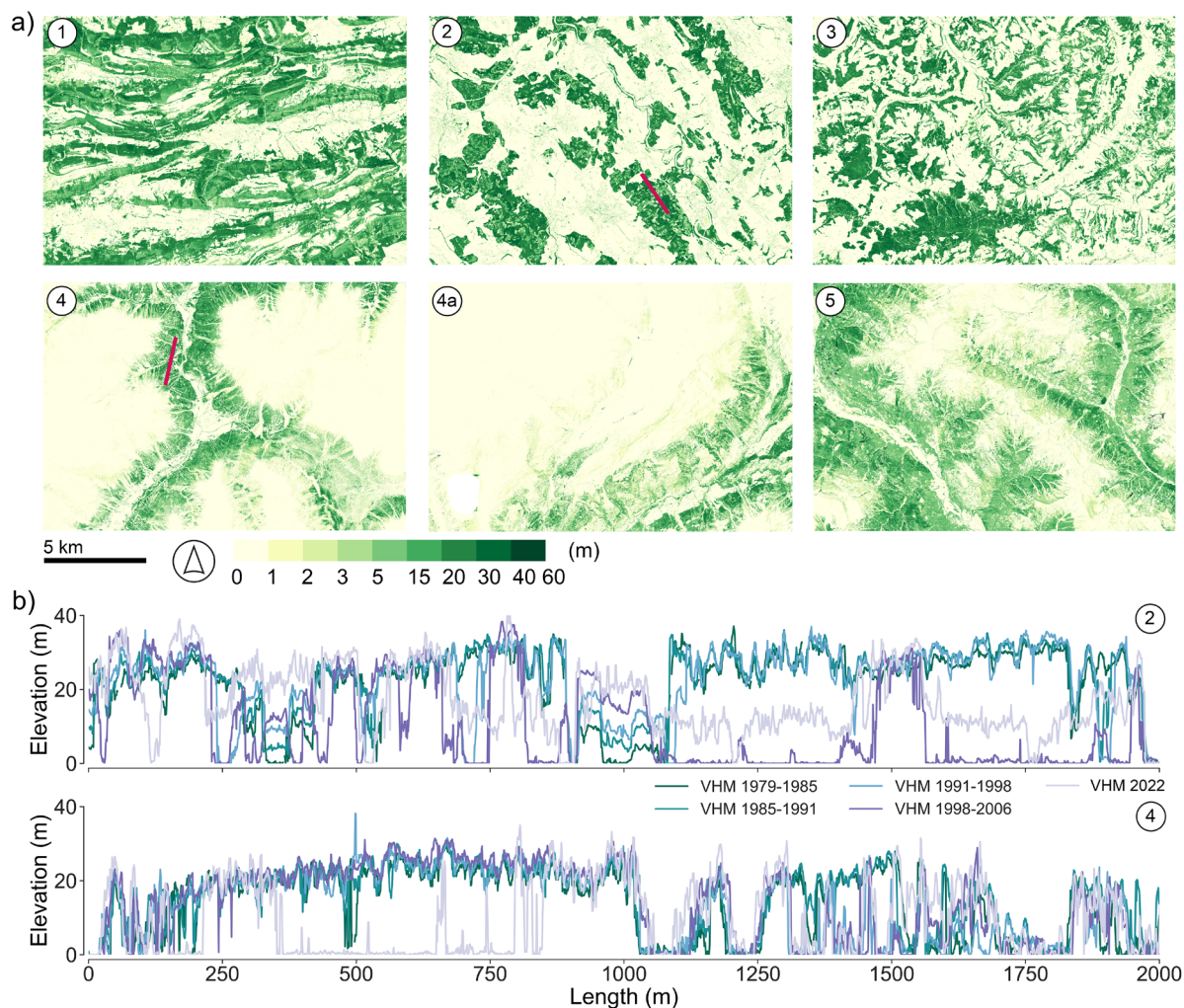


328
329 **Figure 9: Stereo measurements within a Swiss National Forest Inventory (NFI) forest plot on the historical orthophoto of epoch 1**
330 **(left). On the right, a comparison is depicted between the digital surface model (DSM) profile (green line, interval of 1 m) and the**
331 **elevation values of the stereo measurements.**

332 3.4 VHMs and forest change

333 Based on the four countrywide historical DSMs for Switzerland, four VHMs were generated by subtracting a countrywide
334 DTM and applying a non-vegetation mask (see section 2.2.3). Figure 10 shows the VHMs and the forest structure for the six
335 study sites for epoch 2. Since the VHMs are direct derivatives of the DSMs, the statement above about the quality remains
336 valid.

337 Forest dynamics, such as growth, cutting and regrowth between observation epochs are evident over the six study sites, as
338 shown by the height differences of the VHMs between consecutive epochs (Fig. A3). A detailed look at the VHM profiles of
339 study sites 2 and 4 (Fig. 10b) shows minimal change in forest height in mature forest stands (VHM > 20 m), indicating
340 consistency among the VHMs. However, forest growth, cuts or damage followed by regrowth can be detected, for example,
341 between epoch 4 and 2022 (Fig. 10). The Swiss Plateau forest production region, where study site 2 is located, was heavily
342 affected by storm damage. Figure 11 shows a small area of the VHM in region 2 for epochs 1, 3 and 4, overlaid by polygons
343 indicating areas damaged by the two largest storm events recorded in Switzerland: Vivian (25–27 February 1990) and Lothar
344 (26 December 1999). The VHMs effectively capture the storm-affected areas. The VHM of 1982 depicts forest cover in all
345 storm-affected areas, while the 1994 VHM clearly shows the damage caused by storm Vivian. The areas impacted by storm
346 Lothar show mature forest stands in the 1994 VHM, while the heavily damaged areas are visible in the 2002 VHM.



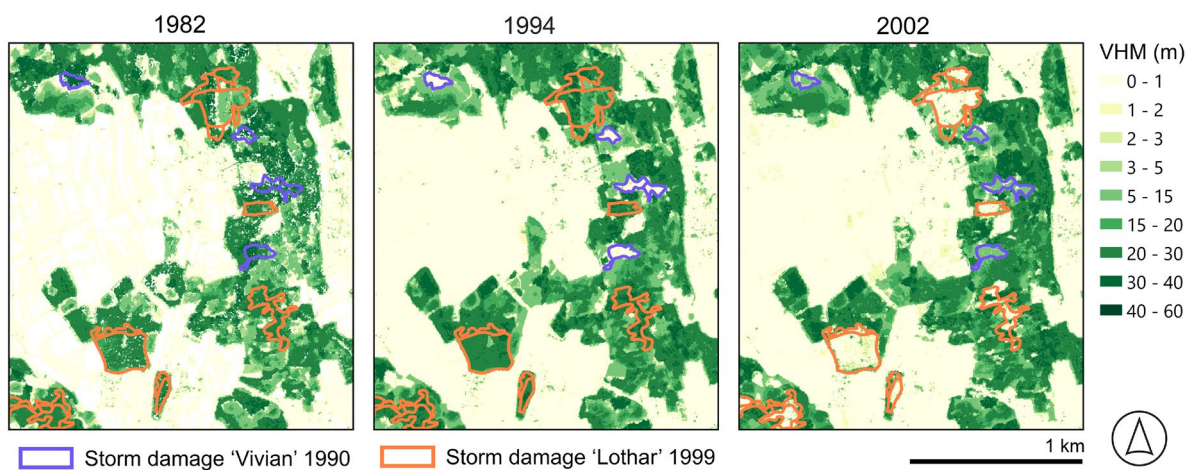
347

348 **Figure 10: Illustration of (a) the vegetation height models (VHM) of epoch 2 (1985–1991) for the six selected study sites. The VHM**
349 **correspond to the years: 1987 for site 1, 1988 for site 2, 1986 for sites 3 and 4a, 1991 for sites 4, and 1989 for site 5. (b) The profile of**
350 **the VHM from historical aerial images for the four epochs and from a modern airborne survey for study sites 2 (acquisition period**
351 **2018 and 2022) and 4 (acquisition period 2022). The 2 km profile line is shown in red in (a).**

352 Besides these qualitative results, these historical VHM have been used in various studies (Price et al., 2020; Ginzler et al.,
353 2021). Ginzler et al. (2021) investigated forest dynamics in Switzerland between 1980 and 2010. Their analysis was based on
354 aggregated average vegetation heights for 100×100 m cells derived from the VHM. They quantified forest dynamics by
355 retrieving the absolute height change over the entire period (sum of absolute differences) and the classified height change
356 between periods (height gain or loss). The results showed high forest dynamics in the Swiss Plateau and some pre-alpine areas
357 in the northern Alps, while significant parts of the Jura and southern Switzerland showed little change during these 30 years.
358 Price et al. (2020) used the historical VHM to map and monitor woody above-ground biomass (AGB) dynamics across



359 Switzerland over 35 years (1983–2017). They found a consistent relationship between vegetation height derived from the
360 VHMs and NFI measures of woody AGB across four inventory periods.



361

362 **Figure 11: Small extent of region 2 (Swiss Plateau), showing the vegetation height models (VHM) of epochs 1, 2 and 4, overlaid by**
363 **polygons indicating areas heavily affected by two major storm events in Switzerland (Vivian: 25 to 27.02.1990 and Lothar:**
364 **26.12.1999).**

365 4 Discussion

366 4.1 Potential of countrywide historical DSMs and VHMs of Switzerland

367 This study underscores the great value of historical aerial images for reconstructing accurate and high-resolution DSMs over
368 approximately three decades. For the epochs 1979–1985, 1985–1991, 1991–1998 and 1998–2006, we successfully processed
369 four countrywide DSMs and VHMs at a resolution of 1 m. The quality of the generated models is sufficient for various
370 geoscience applications, such as the quantification of natural hazards, mass movements, and sediment erosion, and the
371 monitoring of human interference (e.g., deforestation) and urban development. Our historical VHM products show a high level
372 of consistency, suggesting that changes in forest height are real and significant and thus are valuable tools for understanding
373 forest dynamics in Switzerland. This includes the tracking of forest growth and changes in forest cover over time, the
374 differentiation between disturbed (due to management practices or storm events) and undisturbed forests, and the detection of
375 regrowth after disturbance. The clear delineation of storm-damaged areas (e.g., from storms Vivian and Lothar) in our VHM
376 data demonstrates the capability of the models to identify disturbances accurately. By analysing the temporal changes in these
377 areas, we can differentiate between disturbances caused by natural events and those resulting from forest management
378 activities. Therefore, insight can be gained into post-storm regrowth and forest management activities across the forest
379 production regions, and their effectiveness can be quantified, for example in terms of protection forest function. This dataset
380 offers great added value to the Swiss NFI forest management data and supports future management strategies.

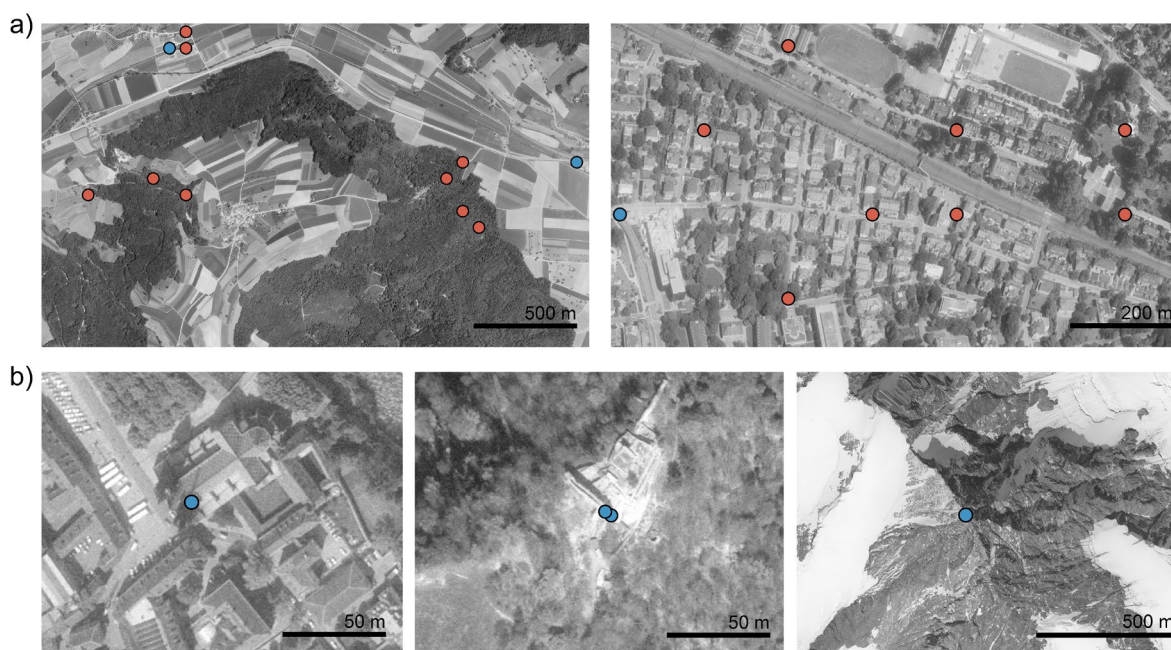


381 4.2 Quality of the DSMs

382 The completeness of the image-matching shows a steady increase over the four epochs (Fig. A2), particularly in areas classified
383 as grasses and herbs. This improvement is strongly related to advancements in camera technology (models and lenses), image-
384 matching results, and the quality of the exterior orientation provided in this study.

385 In areas with successful image-matching, countrywide accuracy analysis comparing derived DSM elevations to swissALTI3D
386 DTM elevations at sealed surface points shows metric to sub-metric accuracy with an uncertainty (NMAD) < 2 m. However,
387 a comparison with geodetic points distributed across Switzerland shows even higher, decametric accuracy.

388 The negative bias, where reference data was lower than the historical DSMs, may have resulted from the suboptimal location
389 of sealed surface points near urban areas and forest edges (Fig. 12a), which could explain the presence of several values more
390 negative than -10 m (Fig. 7b). The comparison with geodetic points shows more positive outliers with values above 10 m (Fig.
391 7c), likely related to the location of reference geodetic points on objects such as rooftops and statues, which cannot be precisely
392 reconstructed from historical photographs (Fig. 12b).



393
394 **Figure 12: Example of suboptimal locations of (a) sealed surface points and (b) geodetic points used for the accuracy assessment.**
395 **Positive biases over these points are shown in blue, whilst negative ones are shown in red.**

396 An elevation bias in areas with slopes greater than 45° and elevations above 3000 m a.s.l. (Fig. 8a, c) is present in many
397 photogrammetric products from airborne and satellite sources (e.g., Piermattei et al., 2019), and is more pronounced in
398 historical images with 8-bit radiometric resolution and lower accuracy in exterior orientation. Steep slopes and mountainous
399 areas often experience strong shadows, overexposed photographs on snow-covered surfaces, and clouds over mountain tops,
400 all affecting image-matching results and vertical accuracy, and increasing noise in the DSMs.



401 Comparing the agreement between manual stereo measurements and the historical DSM of epoch 1, the closed forest land
402 cover class shows the largest bias among all classes. However, similar patterns are visible when comparing manual stereo
403 measurements with a DSM from images acquired by a modern near-infrared Leica ADS Sensor with a GSD of 0.5 m (Ginzler
404 et al., 2015). Ginzler et al. (2015) achieved median values of -0.34 m (coniferous) and -0.79 m (deciduous), with NMAD
405 values in the same range as in this study. The larger bias in historical data might be due to the more demanding visual detection
406 of objects during manual stereo measurements on panchromatic imagery and the coarser resolution of the images. This
407 observation is supported by Ginzler et al. (2015), where stereo measurements on imagery with 0.25 m GSD reduced median
408 values to -0.08 m (coniferous) and 0.16 m (deciduous). All other land cover classes show median values between ~0.1 m and
409 0.7 m and NMAD values between ~1 m and 1.5 m in both studies.

410 **4.3 Challenges of image processing and limitations of our dataset**

411 Challenges in working with airborne historical aerial images can include difficulties accessing the archive, the high cost of
412 images, the low quality of scanning film negatives, and the poor availability of metadata such as exterior and interior
413 orientation. In Switzerland, swisstopo provides free access to a comprehensive archive of scanned historical aerial images
414 covering the entire country, along with calibration protocols and exterior orientation parameters for each image, essential for
415 photogrammetric processing. However, the orientation accuracy of historical images varies between epochs, requiring a
416 vertical correction of the DSMs due to offsets of several metres. Often, historical images lack calibration protocols and exterior
417 orientation information, requiring ground control points to calculate the camera location. This has led the scientific community
418 to adopt ‘structure from motion’ photogrammetric approaches for processing historical aerial images (e.g., Muhammed et al.,
419 2023), as these approaches do not require approximated values, such as camera calibration information. Additionally, pipelines
420 have been developed to minimise the effort of collecting GCPs (e.g., Knuth et al., 2023).

421 To handle a countrywide dataset acquired over three decades, the processing of approximately 40,000 images, as well as post-
422 processing including the vertical correction of about 20,000 DSMs, was done at the map sheet level. Vertical correction was
423 required to minimise offsets caused by an inaccurate exterior orientation of the images (see section 2.2.2). Each corrected map
424 sheet DSM was merged without further consideration of the edges of adjacent map sheets, potentially creating small jumps at
425 the edges. These jumps are negligible at the country scale, but further co-registration should be considered for local and
426 catchment studies involving more than one map sheet.

427 Another challenge of historical black-and-white imagery with 8-bit radiometric resolution is oversaturation in snow-covered
428 or heavily illuminated areas, leading to no or erroneous image-matching results, particularly in mountainous regions. This is
429 evident in the completeness results for points classified as glacial and perpetual snow (see section 3.2). Therefore, for studies
430 related to glaciers and snow, the noise and the voids in the generated DSMs must be addressed with proper void filling and
431 filtering. We used a simple TIN interpolation to fill the voids, providing a binary mask indicating interpolated areas, which
432 can be used to remove these areas for further analysis. For glaciological studies or applications requiring precise dates, we do
433 not have the exact information on the dates of each DSM/pixel, but we provide the year of the survey campaign per map sheet.



434 **5 Data availability**

435 Datasets can be accessed from EnviDat (<https://doi.org/10.16904/envidat.528>, Marty et al., 2024). The following files are
436 available for the four epochs: countrywide digital surface model (DSM), hillshaded DSM, and vegetation height models
437 (VHMs). A metadata shapefile is provided with information about the acquisition year of the photographs used here; the
438 geometry corresponds to the 1:25,000 map sheets used during this study. In addition, a binary raster is provided indicating
439 successfully matched pixels (1) and interpolated pixels (0), and a non-vegetation mask raster ‘TLM_Vegetation_mask’ is
440 provided, indicating vegetated areas (1) and non-vegetated areas (0). All the raster files are provided as GeoTIFF files.

441 **6 Conclusions**

442 Millions of aerial photographs dating from the First World War to the early 2000s represent an enormous, yet largely untapped,
443 resource for geoscientists, with significant potential for documenting and quantifying surface changes over the last century. In
444 this study, we used freely available historical stereo images covering the whole of Switzerland, processed using
445 photogrammetric software. These images were provided with both exterior and interior orientation, allowing us to derive four
446 countrywide DSMs at a 1 m spatial resolution across four epochs, with survey campaigns spanning approximately seven years.
447 Our developed workflow achieved sub-metric accuracy and high completeness of the DSMs in nearly all regions of
448 Switzerland, demonstrating the feasibility of capturing continuous surface change patterns at a high spatial resolution over
449 different land cover classes. However, lower completeness and increased noise were present in snow-covered areas, due to
450 image saturation and reduced performance of the image-matching algorithm in these areas. As our study was conducted as part
451 of the Swiss NFI, we also generated four countrywide VHMs using an available countrywide DTM. These VHMs have been
452 used to quantify forest changes (Ginzler et al., 2021) and monitor above-ground biomass (Price et al., 2020). The high
453 consistency of the VHMs indicates their potential for future research into forest ecosystem dynamics, services and
454 management.

455 Future work can build upon these datasets by integrating modern data to extend the observation period, thereby enhancing the
456 detection of climate signals. Additionally, refining time series methods for very-high-resolution datasets will further improve
457 our understanding of surface changes and related processes.

458 Finally, this study highlights the importance of recognising the value of historical aerial imagery datasets. We urge mapping
459 agencies, governmental authorities and military services to unlock these archives and make them freely accessible online. The
460 creation of countrywide historical aerial image DSMs is feasible only when such data is readily available, as demonstrated by
461 the open access provided by swisstopo in Switzerland.

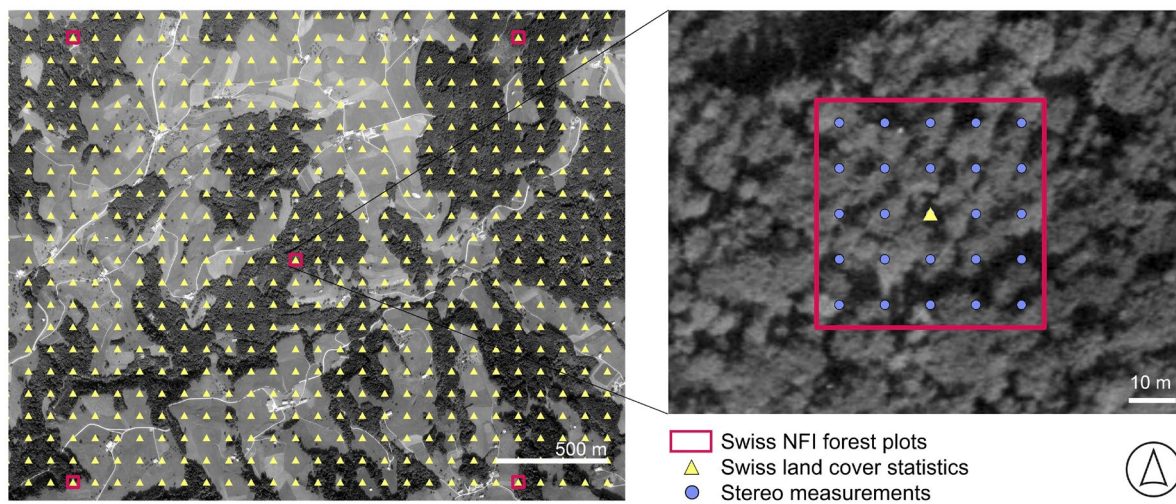
462

463

464

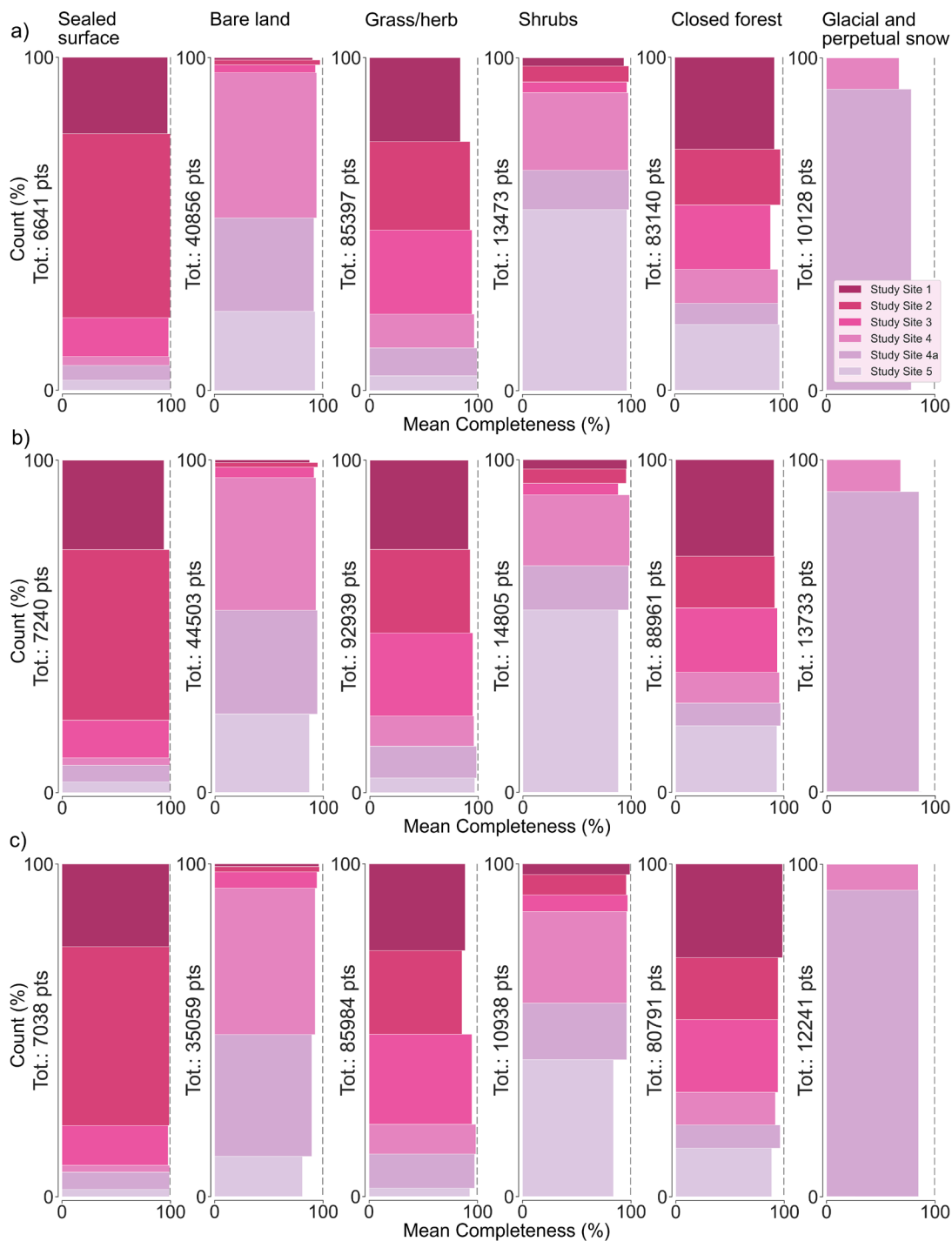


465 **Appendix A**



466

467 **Figure A1: Illustration of the distribution of the Swiss land cover statistic points and the Swiss National Forest Inventory (NFI)**
468 **forest plots with the stereo measurements. The background is the generated orthophoto from the first epoch (1979–1985).**



469

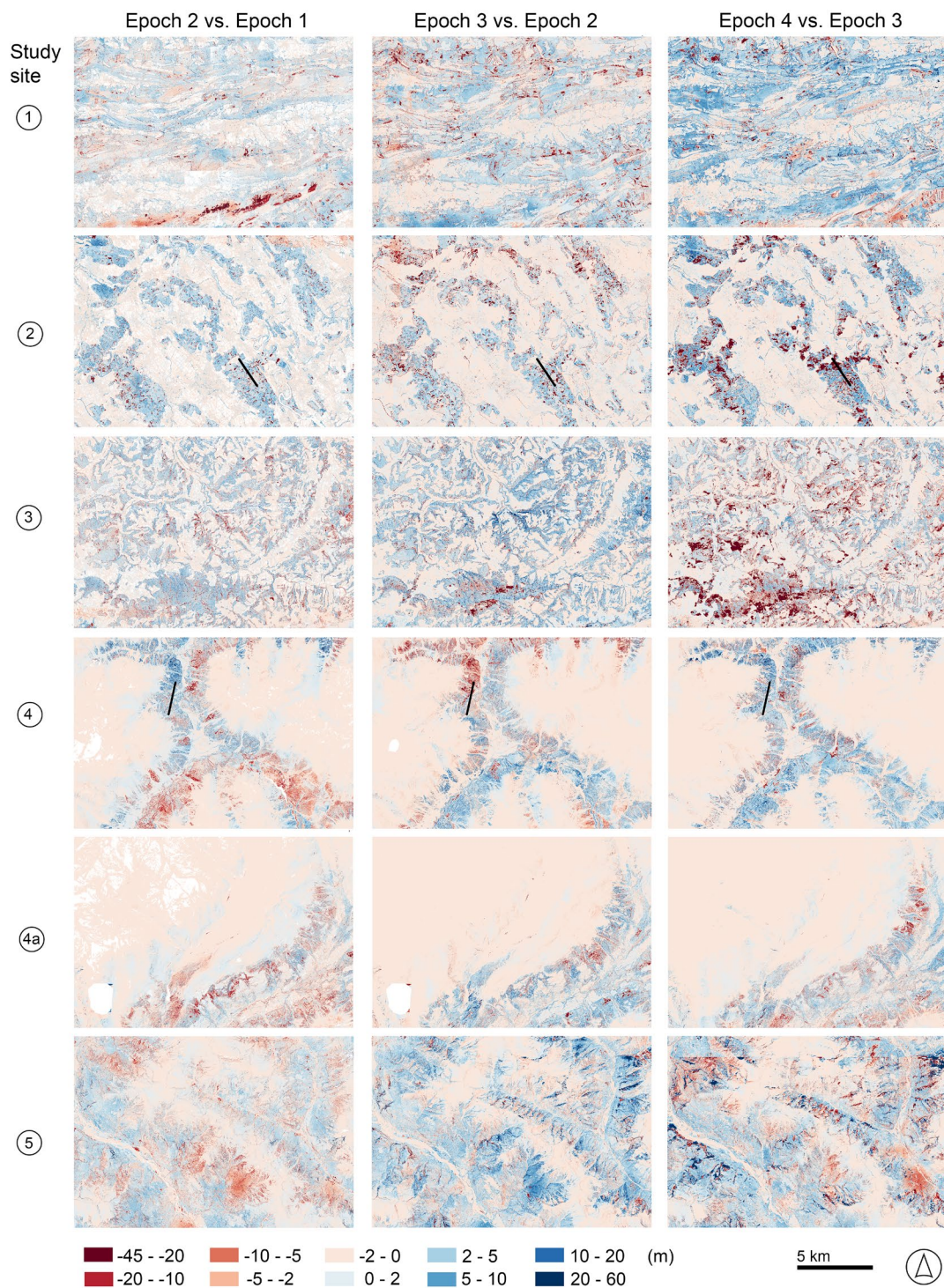
470 **Figure A2: Distribution of the mean completeness values, as percentages, for (a) epoch 2, (b) epoch 3, and (c) epoch 4, across the six**
 471 **study sites and the six land cover classes – sealed surface, bare land, grass/herb, shrub, closed forest, and glacial and perpetual snow.**
 472 **The last class is only present in study sites 4, 4a and 5.**



473 **Table A1: Mean completeness values (as percentages) for each epoch over the six study sites, and for the six land cover classes. For**
 474 **each class, the number of points used to assess the accuracy is provided. n.a. indicates not available.**

Study site	Sealed surface		Bare land		Grass/herb		Shrub		Closed forest		Glacial and perpetual snow	
	Mean (%)	Count (No.)	Mean (%)	Count (No.)	Mean (%)	Count (No.)	Mean (%)	Count (No.)	Mean (%)	Count (No.)	Mean (%)	Count (No.)
Epoch 1												
1	95	1312	84	221	53	17428	87	286	84	17899	n.a.	n.a.
2	98	3416	86	565	58	19879	92	586	93	12254	n.a.	n.a.
3	97	726	91	1172	74	20202	94	409	88	14877	n.a.	n.a.
4	99	173	95	19892	99	8785	99	3244	96	8496	51	1543
4a	99	284	94	12759	91	8119	98	1838	98	5346	64	9774
5	100	190	94	9045	99	3550	95	7125	98	15193	82	18
Epoch 2												
1	97	1526	90	287	84	21520	93	331	92	22974	n.a.	n.a.
2	99	3669	97	606	93	22699	98	646	97	13934	n.a.	n.a.
3	98	776	93	956	94	21609	96	434	88	16075	n.a.	n.a.
4	99	176	94	17811	96	8638	98	3139	95	8477	67	951
4a	100	296	92	11497	99	7163	98	1593	95	5287	78	9155
5	100	198	93	9699	99	3768	96	7330	97	16393	76	22
Epoch 3												
1	94	1947	87	342	91	24952	96	408	91	25816	n.a.	n.a.
2	99	3718	95	618	92	23317	95	639	92	13841	n.a.	n.a.
3	98	819	91	1400	95	23259	88	514	94	17229	n.a.	n.a.
4	99	163	93	17761	96	8437	98	3158	96	8239	68	1312
4a	99	360	94	13907	98	8868	98	1964	97	6060	85	12399
5	100	233	87	10475	97	4106	88	8122	94	17776	87	22
Epoch 4												
1	99	1748	96	281	89	22408	99	348	98	22718	n.a.	n.a.
2	99	3784	97	560	86	21622	96	670	94	15078	n.a.	n.a.
3	98	840	94	1715	95	23288	97	553	94	17637	n.a.	n.a.
4	99	147	93	15428	98	7680	96	3008	92	7927	85	953
4a	99	365	90	12840	97	8811	96	1862	96	5623	85	11283
5	99	154	81	4235	93	2175	84	4497	88	11808	27	5

475



476

477 **Figure A3: The height difference between the vegetation height models (VHM) of consecutive epochs for each study site (1–5). The**
 478 **black line in study sites 2 and 4 indicates the location of the profile shown in Figure 10.**



479 **Supplement**

480 No supplemental material.

481 **Author Contributions**

482 MM and CG designed the study. MM processed and generated all the data. LP and MM analysed the dataset. LP prepared all
483 the figures and tables. LP and MM wrote the manuscript. All authors contributed to the discussion and editing of the text.

484 **Competing interests**

485 The authors declare that they have no conflicts of interest.

486 **Acknowledgements**

487 This study was supported by the Swiss National Forest Inventory (NFI). We thank the Federal Statistical Office FSO and the
488 Federal Office of Topography swisstopo for providing access to the historical photographs. We are grateful to Holger Heisig
489 (swisstopo) for the successful semi-automatic orientation of thousands of historical images and fruitful and interesting
490 discussions about this source of data and to Dr Melissa Dawes for professional language editing.

491 **Funding**

492 This study was carried out in the framework of the Swiss National Forest Inventory (NFI), a cooperative effort between the
493 Swiss Federal Institute for Forest, Snow and Landscape Research (WSL) and the Swiss Federal Office for the Environment
494 (FOEN).

495 **References**

496 Abegg, M., Bösch, R., Kükenbrink, D., and Morsdorf, F.: Tree volume estimation with terrestrial laser scanning—testing for
497 bias in a 3D virtual environment, *Agric. For. Meteorol.*, 331, 109348, <https://doi.org/10.1016/j.agrformet.2023.109348>, 2023.
498
499 Belart, J.M., Magnússon, E., Berthier, E., Gunnlaugsson, Á.Þ., Pálsson, F., Aðalgeirsdóttir, G., Jóhannesson, T., Thorsteinsson,
500 T., and Björnsson, H.: Mass balance of 14 Icelandic glaciers, 1945–2017: spatial variations and links with climate, *Front. Earth
501 Sci.*, 8, 163, <https://doi.org/10.3389/feart.2020.00163>, 2020.
502



- 503 Berveglieri, A., Imai, N.N., Tommaselli, A.M., Casagrande, B. and Honkavaara, E.: Successional stages and their evolution
504 in tropical forests using multi-temporal photogrammetric surface models and superpixels, ISPRS-J. Photogramm. Remote
505 Sens., 146, 548-558, <https://doi.org/10.1016/j.isprsjprs.2018.11.002>, 2018.
- 506
- 507 Berveglieri, A., Tommaselli, A.M.G., Imai, N.N., Ribeiro, E.A.W., Guimaraes, R.B. and Honkavaara, E.: Identification of
508 successional stages and cover changes of tropical forest based on digital surface model analysis, IEEE J. Sel. Top. Appl. Earth
509 Obs. Remote Sens., 9(12), 5385-5397, <https://doi.org/10.1109/JSTARS.2016.2606320>, 2016.
- 510
- 511 BFS. Bundesamt für Statistik, Arealstatistik Schweiz – Nomenklatur 2004.
512 <https://www.bfs.admin.ch/bfs/de/home/statistiken/raum-umwelt/nomenklaturen/arealstatistik.html>, last access: 29 August
513 2024.
- 514
- 515 Bolles, K.C. and Forman, S.L.: Evaluating landscape degradation along climatic gradients during the 1930s dust bowl drought
516 from panchromatic historical aerial photographs, United States Great Plains. Front. Earth Sci., 6, 153,
517 <https://doi.org/10.3389/feart.2018.00153>, 2018.
- 518
- 519 Božek, P., Janus, J. and Mitka, B.: Analysis of changes in forest structure using point clouds from historical aerial photographs,
520 Remote Sens., 11(19), p.2259, <https://doi.org/10.3390/rs11192259>, 2019.
- 521
- 522 Cusicanqui, D., Rabatel, A., Vincent, C., Bodin, X., Thibert, E., and Francou, B.: Interpretation of volume and flux changes
523 of the Laurichard rock glacier between 1952 and 2019, French Alps, J. Geophys. Res. Earth Surf., 126(9), p.e2021JF006161,
524 <https://doi.org/10.1029/2021JF006161>, 2021.
- 525
- 526 DeVenecia K., Walker S, and Bingcai, Z.: New Approaches to Generating and Processing High Resolution Elevation Data
527 with Imagery, Photogrammetric Week '07, 297-308, Wichmann Verlag, Heidelberg, 2007.
- 528
- 529 Denzinger, F., Machguth, H., Barandun, M., Berthier, E., Girod, L., Kronenberg, M., Usubaliev, R., and Hoelzle, M.: Geodetic
530 mass balance of Abramov Glacier from 1975 to 2015, J. Glaciol., 67(262), 331-342, <http://doi.org/10.1017/jog.2020.108>,
531 2021.
- 532
- 533 Fleischer, F., Haas, F., Piermattei, L., Pfeiffer, M., Heckmann, T., Altmann, M., Rom, J., Stark, M., Wimmer, M.H., Pfeifer,
534 N., and Becht, M.: Multi-decadal (1953–2017) rock glacier kinematics analysed by high-resolution topographic data in the
535 upper Kaunertal, Austria, Cryosphere, 15(12), 5345-5369, <https://doi.org/10.5194/tc-15-5345-2021>, 2021.
- 536



- 537 Geyman, E.C., J. J. van Pelt, W., Maloof, A.C., Faste Aas, H., and Kohler, J.: Historical glacier change on Svalbard predicts
538 doubling of mass loss by 2100, *Nature*, 601, 374–379, <https://doi.org/10.1038/s41586-021-04314-4>, 2022.
539
- 540 Ginzler, C. and Hobi, M.L.: Countrywide stereo-image matching for updating digital surface models in the framework of the
541 Swiss National Forest Inventory, *Remote Sens.*, 7, 4343–4370, <https://doi.org/10.3390/rs70404343>, 2015.
542
- 543 Ginzler, C., Price, B., Weber, D., Hobi, M., and Marty, M.: Dynamik der Vegetationshöhen im Schweizer Wald, *Swiss Forestry*
544 *J.*, 172(5), 310–317, <https://doi.org/10.3188/szf.2021.0310>, 2021.
545
- 546 Gomez, C., Hayakawa, Y., and Obanawa, H.: A study of Japanese landscapes using structure from motion derived DSMs and
547 DEMs based on historical aerial photographs: New opportunities for vegetation monitoring and diachronic geomorphology,
548 *Geomorphology*, 242, 11–20, <https://doi.org/10.1016/j.geomorph.2015.02.021>, 2015.
549
- 550 Heisig, H. and Simmen, J.L.: Re-engineering the past: countrywide geo-referencing of archival aerial imagery, *J. Photogramm.*
551 *Remote Sens. Geoinf. Sci.*, 89(6), 487–503, <https://doi.org/10.1007/s41064-021-00162-z>, 2021.
552
- 553 Höhle, J. and Höhle, M.: Accuracy assessment of digital elevation models by means of robust statistical methods, *ISPRS-J.*
554 *Photogramm. Remote Sens.*, 64(4), 398–406, <https://doi.org/10.1016/j.isprsjprs.2009.02.003>, 2009.
555
- 556 Hufkens, K., de Haulleville, T., Kearsley, E., Jacobsen, K., Beekman, H., Stoffelen, P., Vandeloos, F., Meeus, S., Amara,
557 M., Van Hirtum, L., and Van den Bulcke, J.: Historical aerial surveys map long-term changes of forest cover and structure in
558 the Central Congo Basin, *Remote Sens.*, 12(4), 638, <https://doi.org/10.3390/rs12040638>, 2020.
559
- 560 Hudak, A.T. and Wessman, C.A.: Textural analysis of historical aerial photography to characterise woody plant encroachment
561 in South African Savanna, *Remote Sens. Environ.*, 66(3), 317–330, [https://doi.org/10.1016/S0034-4257\(98\)00078-9](https://doi.org/10.1016/S0034-4257(98)00078-9), 1998.
562
- 563 Kadmon, R. and Harari-Kremer, R.: Studying long-term vegetation dynamics using digital processing of historical aerial
564 photographs, *Remote Sens. Environ.*, 68(2), 164–176, [https://doi.org/10.1016/S0034-4257\(98\)00109-6](https://doi.org/10.1016/S0034-4257(98)00109-6), 1999.
565
- 566 Knuth, F., Shean, D., Bhushan, S., Schwat, E., Alexandrov, O., McNeil, C., Dehecq, A., Florentine, C., and O’Neel, S.:
567 Historical Structure from Motion (HSfM): Automated processing of historical aerial photographs for long-term topographic
568 change analysis, *Remote Sens. Environ.* 285, 113379, <https://doi.org/10.1016/j.rse.2022.113379>, 2023.
569



- 570 Korsgaard, N.J., Nuth, C., Khan, S.A., Kjeldsen, K.K., Bjørk, A.A., Schomacker, A., and Kjær, K.H.: Digital elevation model
571 and orthophotographs of Greenland based on aerial photographs from 1978–1987, *Sci. Data*, 3, 160032,
572 <https://doi.org/10.1038/sdata.2016.32>, 2016.
- 573
- 574 Kulha, N., Pasanen, L., and Aakala, T.: How to calibrate historical aerial photographs: a change analysis of naturally dynamic
575 boreal forest landscapes, *Forests*, 9(10), 631, <https://doi.org/10.3390/f9100631>, 2018.
- 576
- 577 Kupidura, P., Osińska-Skotak, K., Lesisz, K., and Podkowa, A.: The efficacy analysis of determining the wooded and shrubbed
578 area based on archival aerial imagery using texture analysis, *ISPRS Int. J. Geo-Inf.*, 8(10), 450,
579 <https://doi.org/10.3390/ijgi8100450>, 2019.
- 580
- 581 Marty, M., Piermattei, L., Ginzler, C., and Waser, L.T.: Countrywide DSM and VHM from historical aerial images, *Envidar*
582 [data set], <https://doi.org/10.16904/envidat.528>, 2024.
- 583
- 584 Magnússon, E., Muñoz-Cobo Belart, J., Pálsson, F., Ágústsson, H., and Crochet, P.: Geodetic mass balance record with
585 rigorous uncertainty estimates deduced from aerial photographs and lidar data – case study from Drangajökull ice cap, NW
586 Iceland, *Cryosphere*, 10(1), 159-177, <https://doi.org/10.5194/tc-10-159-2016>, 2016.
- 587
- 588 Micheletti, N., Lane, S.N., and Chandler, J.H.: Application of archival aerial photogrammetry to quantify climate forcing of
589 alpine landscapes, *Photogram. Rec.*, 30, 143-165, <https://doi.org/10.1111/phor.12099>, 2015.
- 590
- 591 Morgan, J.L. and Gergel, S.E.: Quantifying historic landscape heterogeneity from aerial photographs using object-based
592 analysis, *Landscape Ecol.*, 25, 985-998, <https://doi.org/10.1007/s10980-010-9474-1>, 2010.
- 593
- 594 Muhammed, M.A., Hailu, B.T., Mische, G., Wraase, L., Nauss, T. and, Zeuss, D.: High-resolution digital elevation models and
595 orthomosaics generated from historical aerial photographs (since the 1960s) of the Bale Mountains in Ethiopia, *Earth Syst.*
596 *Sci. Data*, 15(12), 5535-5552, <https://doi.org/10.5194/essd-15-5535-2023>, 2023.
- 597
- 598 Nebiker, S., Lack, N., and Deuber, M.: Building change detection from historical aerial photographs using dense image
599 matching and object-based image analysis, *Remote Sens.*, 6(9), 8310-8336, <https://doi.org/10.3390/rs6098310>, 2014.
- 600
- 601 Nurminen, K., Litkey, P., Honkavaara, E., Vastaranta, M., Holopainen, M., Lyytikäinen-Saarenmaa, P., Kantola, T., and
602 Lyytikäinen, M.: Automation aspects for the georeferencing of photogrammetric aerial image archives in forested scenes,
603 *Remote Sens.*, 7(2), 1565-1593, <https://doi.org/10.3390/rs70201565>, 2015.



604
605 Peppas, M.V., Mills, J.P., Fieber, K.D., Haynes, I., Turner, S., Turner, A., Douglas, M., and Bryan, P.G.: Archaeological feature
606 detection from archive aerial photography with a SfM-MVS and image enhancement pipeline, *Int. arch.*
607 *Photogramm. Remote Sens. Spat. Inf. Sci.*, 42, 869-875, <https://doi.org/10.5194/isprs-archives-XLII-2-869-2018>, 2018.
608
609 Piermattei, L., Heckmann, T., Betz-Nutz, S., Altmann, M., Rom, J., Fleischer, F., Stark, M., Haas, F., Ressler, C., Wimmer,
610 M.H., and Pfeifer, N.: Evolution of an Alpine proglacial river during 7 decades of deglaciation, *Earth Surf. Dyn.*, 11(3), 383-
611 403, <https://doi.org/10.5194/esurf-11-383-2023>, 2023.
612
613 Piermattei, L., Marty, M., Ginzler, C., Pöchtrager, M., Karel, W., Ressler, C., Pfeifer, N., and Hollaus, M.: Pléiades satellite
614 images for deriving forest metrics in the Alpine region, *Int. J. Appl. Earth Obs. Geoinf.*, 80, 240-256,
615 <https://doi.org/10.1016/j.jag.2019.04.008>, 2019.
616
617 Price, B., Waser, L.T., Wang, Z., Marty, M., Ginzler, C. and Zellweger, F.: Predicting biomass dynamics at the national extent
618 from digital aerial photogrammetry, *Int. J. Appl. Earth Obs. Geoinf.*, 90, 102116, <https://doi.org/10.1016/j.jag.2020.102116>,
619 2020.
620
621 Risbøl, O., Briese, C., Doneus, M., and Nesbakken, A.: Monitoring cultural heritage by comparing DEMs derived from
622 historical aerial photographs and airborne laser scanning, *J. Cult. Herit.*, 16(2), 202-209,
623 <https://doi.org/10.1016/j.culher.2014.04.002>, 2015.
624
625 Schwab, E., Istanbuloglu, E., Horner-Devine, A., Anderson, S., Knuth, F., and Shean, D.: Multi-decadal erosion rates from
626 glacierized watersheds on Mount Baker, Washington, USA, reveal topographic, climatic, and lithologic controls on sediment
627 yields, *Geomorphology*, 438, 108805, <https://doi.org/10.1016/j.geomorph.2023.108805>, 2023.
628
629 Swisstopo, swissALTI3D version 2017: [https://backend.swisstopo.admin.ch/fileservice/sdweb-docs-prod-swisstopoch-](https://backend.swisstopo.admin.ch/fileservice/sdweb-docs-prod-swisstopoch-files/files/2023/11/14/cf4990a1-6bfb-4331-b990-a894d686266e.pdf)
630 [files/files/2023/11/14/cf4990a1-6bfb-4331-b990-a894d686266e.pdf](https://backend.swisstopo.admin.ch/fileservice/sdweb-docs-prod-swisstopoch-files/files/2023/11/14/cf4990a1-6bfb-4331-b990-a894d686266e.pdf), last access: 29 August 2024, 2017.
631
632 Swisstopo geodetic points: <https://opendata.swiss/en/dataset/lagefixpunkte-lfp1-landesvermessung>, last access: 29 August
633 2024, 2023.
634
635 Swisstopo, aerial photographs: <https://www.swisstopo.admin.ch/en/analogue-aerial-photographs>, last access: 29 August 2024,
636 2024a.
637



- 638 Swisstopo, National Map 1:25'000: <https://www.swisstopo.admin.ch/en/national-map-1-25000>, last access: 29 August 2024,
639 2024b.
640
- 641 Swisstopo, swissALTI3D technical information: <https://www.swisstopo.admin.ch/en/height-model-swissalti3d>, last access: 29
642 August 2024, 2024c.
643
- 644 Swisstopo, The topographic Landscape Model TLM: [https://www.swisstopo.admin.ch/en/information-topographic-landscape-](https://www.swisstopo.admin.ch/en/information-topographic-landscape-model)
645 [model](https://www.swisstopo.admin.ch/en/information-topographic-landscape-model), last access: 29 August 2024, 2024d.
646
- 647 Vastaranta, M., Niemi, M., Wulder, M.A., White, J.C., Nurminen, K., Litkey, P., Honkavaara, E., Holopainen, M., and Hyypä,
648 J.: Forest stand age classification using time series of photogrammetrically derived digital surface models, *Scand. J. For. Res.*,
649 31(2), 194-205, <https://doi.org/10.1080/02827581.2015.1060256>, 2016.
650
- 651 Véga, C. and St-Onge, B.: Height growth reconstruction of a boreal forest canopy over a period of 58 years using a combination
652 of photogrammetric and lidar models, *Remote Sens. Environ.*, 112(4), 1784-1794, <https://doi.org/10.1016/j.rse.2007.09.002>,
653 2008.
654
- 655 Wang, Z., Ginzler, C., Eben, B., Rehus, N., and Waser, L.T.: Assessing changes in mountain treeline ecotones over 30 years
656 using CNNs and historical aerial images, *Remote Sens.*, 14, 2135, <https://doi.org/10.3390/rs14092135>, 2022.
657
- 658 Waser, L.T., Baltsavias, E., Ecker, K., Eisenbeiss, H., Ginzler, C., Kuchler, M., Thee, P., and Zhang, L.: High-resolution digital
659 surface models (DSMs) for modelling fractional shrub/tree cover in a mire environment, *Int. J. Remote Sens.*, 29(5), 1261-
660 1276, <https://doi.org/10.1080/01431160701736422>, 2008a.
661
- 662 Waser, L.T., Baltsavias, E., Ecker, K., Eisenbeiss, H., Feldmeyer-Christe, E., Ginzler, C., and Zhang, L.: Assessing changes
663 of forest area and shrub encroachment in a mire ecosystem using digital surface models and CIR aerial images, *Remote Sens.*
664 *Environ.*, 112(5), 1956-1968, <https://doi.org/10.1016/j.rse.2007.09.015>, 2008b.
665
- 666 Waser, L.T., Fischer, C., Wang, Z., and Ginzler, C.: Wall-to-wall forest mapping based on digital surface models from image-
667 based point clouds and a NFI forest definition, *Forests*, 6, 4510–4528, <https://doi.org/10.3390/f6124386>, 2015.
668
669
670